

University of Windsor

## Scholarship at UWindor

---

Electronic Theses and Dissertations

Theses, Dissertations, and Major Papers

---

1-1-1984

### Calculations of Lamb shifts in muonic atoms.

Louis Lee Byer  
*University of Windsor*

Follow this and additional works at: <https://scholar.uwindsor.ca/etd>

---

#### Recommended Citation

Byer, Louis Lee, "Calculations of Lamb shifts in muonic atoms." (1984). *Electronic Theses and Dissertations*. 6783.

<https://scholar.uwindsor.ca/etd/6783>

This online database contains the full-text of PhD dissertations and Masters' theses of University of Windsor students from 1954 forward. These documents are made available for personal study and research purposes only, in accordance with the Canadian Copyright Act and the Creative Commons license—CC BY-NC-ND (Attribution, Non-Commercial, No Derivative Works). Under this license, works must always be attributed to the copyright holder (original author), cannot be used for any commercial purposes, and may not be altered. Any other use would require the permission of the copyright holder. Students may inquire about withdrawing their dissertation and/or thesis from this database. For additional inquiries, please contact the repository administrator via email ([scholarship@uwindsor.ca](mailto:scholarship@uwindsor.ca)) or by telephone at 519-253-3000ext. 3208.

CALCULATIONS OF LAMB SHIFTS IN MUONIC ATOMS

by

Louis Lee Byer

A Thesis

Submitted to the Faculty of Graduate Studies through the  
Department of Physics in Partial Fulfillment of the  
Requirements for the Degree of Master of  
Science at the University of Windsor  
Windsor, Ontario

1984

UMI Number: EC54769

### INFORMATION TO USERS

The quality of this reproduction is dependent upon the quality of the copy submitted. Broken or indistinct print, colored or poor quality illustrations and photographs, print bleed-through, substandard margins, and improper alignment can adversely affect reproduction.

In the unlikely event that the author did not send a complete manuscript and there are missing pages, these will be noted. Also, if unauthorized copyright material had to be removed, a note will indicate the deletion.

**UMI<sup>®</sup>**

---

UMI Microform EC54769  
Copyright 2010 by ProQuest LLC  
All rights reserved. This microform edition is protected against  
unauthorized copying under Title 17, United States Code.

---

ProQuest LLC  
789 East Eisenhower Parkway  
P.O. Box 1346  
Ann Arbor, MI 48106-1346

© Louis Lee Byer 1984

799351

## ACKNOWLEDGEMENTS

I would like to thank Dr. G.W.F. Drake for his valuable time in directing me through this work.

I would also like to thank Debbie Actomick for some of the numerical groundwork necessary for this work and the many members of the Physics department with whom I was able to exchange ideas. In particular I would like to thank my wife and parents for their continued support.

Abstract

Muon-atomic systems are of interest because of the important role played by quantum electrodynamic (QED) effects as compared with electronic systems with the same nuclear charge. The QED corrections to the energy levels consist primarily of nuclear vacuum polarization and muon self-energy effects. The differences in energy levels  $2s_{\frac{1}{2}} - 2p_{\frac{1}{2},\frac{3}{2}}$  are particularly sensitive to QED and finite nuclear size effects.

This work describes the calculation of the energy levels  $1s_{\frac{1}{2}}, 2s_{\frac{1}{2}}, 2p_{\frac{1}{2}}, 2p_{\frac{3}{2}}$  and the energy differences  $2s_{\frac{1}{2}} - 2p_{\frac{1}{2},\frac{3}{2}}$  of the muonic systems  $\mu^- - H_1^+$ ,  $\mu^- - H_2^+$ ,  $\mu^- - He_4^{++}$ ,  $\mu^- - Li_6^{3+}$  and  $\mu^- - Be_9^{4+}$  by direct numerical integration of the Dirac equation. The results for the energy differences are used to identify cases which might be accessible to experimental measurement.

Although the splittings nominally scale as  $Z^4$ , cancellations between the vacuum polarization and finite nuclear size terms bring some of the transitions for  $\mu^- - Li_6^{3+}$  and  $\mu^- - Be_9^{4+}$  into the range covered by tunable dye lasers. A measurement of the transition frequencies would provide a more precise determination of the nuclear radii than is currently available.

TABLE OF CONTENTS

ABSTRACT..... i

LIST OF TABLES..... iii

LIST OF GRAPHS..... iv

LIST OF FIGURES..... v

SECTIONS

1. INTRODUCTION..... 1

2. THEORETICAL DESCRIPTION..... 6

    2.1 Centre of Mass Motion..... 7

    2.2 Dirac Equation..... 8

    2.3 Perturbation Calculations..... 12

    2.4 Finite Nuclear Size..... 13

    2.5 Leading Order Vacuum Polarization..... 14

    2.6  $\alpha^2 Z\alpha$  Vacuum Polarization Potential..... 21

    2.7 Muon Self Energy..... 22

    2.8 Calculation of Energy Levels..... 24

    2.9 Other Corrections..... 25

    2.10 Orders of Magnitude..... 27

3. RESULTS..... 31

    3.1 Tables & Graphs..... 33

    3.2 Computational Procedures and Error  
        Discussions..... 47

    3.3 Discussion of Results..... 50

4. CONCLUSIONS AND DISCUSSIONS..... 52

A. APPENDIX ..... 55

    A.1 Romberg Integration..... 55

    A.2 Interpolating Polynomials..... 56

    A.3 Numerical Solutions to First Order Coupled  
        Differential Equations..... 58

REFERENCES..... 61

LIST OF TABLES

Vector Coupling Coefficients.....10

Dirac Energy Eigenvalues due to  $\alpha Z\alpha$  Vacuum  
Polarization and Finite Size Coulomb Potentials.....33

$2s_{\kappa} - 2p_{\kappa, \frac{3}{2}}$  Energy Differences due to Vacuum  
Polarization and Finite Size Coulomb Potentials.....34

Perturbation Calculations of the  $\alpha Z\alpha$  Vacuum  
Polarization Correction.....35

Perturbation Calculations of the Muon  
Self Energy Correction.....35

Total  $E(2s_{\kappa} - 2p_{\kappa, \frac{3}{2}})$  Energy Splittings and  
Their Associated Wavelengths.....36

$E(2p_{\frac{3}{2}}) - E(2p_{\frac{1}{2}})$  Energy Differences.....36

Methods Used in the Determination of Uncertainties.....37

LIST OF GRAPHS

Graph 3.1.1	$\text{Be}_9$	$1s_{\frac{1}{2}}$	Unnormalized $G(r)$ vs $r$	.....	39
Graph 3.1.2	$\text{Be}_9$	$1s_{\frac{1}{2}}$	Unnormalized $F(r)$ vs $r$	.....	40
Graph 3.1.3	$\text{Be}_9$	$2s_{\frac{1}{2}}$	Unnormalized $G(r)$ vs $r$	.....	41
Graph 3.1.4	$\text{Be}_9$	$2s_{\frac{1}{2}}$	Unnormalized $F(r)$ vs $r$	.....	42
Graph 3.1.5	$\text{Be}_9$	$2p_{\frac{1}{2}}$	Unnormalized $G(r)$ vs $r$	.....	43
Graph 3.1.6	$\text{Be}_9$	$2p_{\frac{1}{2}}$	Unnormalized $F(r)$ vs $r$	.....	44
Graph 3.1.7	$\text{Be}_9$	$2p_{\frac{3}{2}}$	Unnormalized $G(r)$ vs $r$	.....	45
Graph 3.1.8	$\text{Be}_9$	$2p_{\frac{3}{2}}$	Unnormalized $F(r)$ vs $r$	.....	46

LIST OF FIGURES

Figure 1.1	Energy Level Diagram for $\mu^- - \text{He}_4^{++}$	..... 5
Figure 2.1.1	Illustrating Centre of Mass and Relative Coordinates	..... 7
Figure 2.5.1	$\propto \alpha$ Vacuum Polarization Potential	.....14
Figure 2.5.2	Electron Positron Scattering in the Field of the Leading Order Vacuum Polarization Potential	.....15
Figure 2.5.3	Electron Positron Scattering via the Coulomb Interaction	.....16
Figure 2.5.4	Expansion of the Exact Photon Propogator	.....16
Figure 2.6.1	$\propto^2 \propto$ Vacuum Polarization Potential	.....21
Figure 2.7.1	$\propto \propto$ Muon Self Energy	.....22
Figure 2.7.2	Expansion of the Exact Muon Propogator	.....23
Figure 2.9.1	Observation Point P Outside a Discrete Nuclear Charge Distribution	.....25
Figure 2.10.1	Muon Scattering via the Coulomb Interaction	.....28

## 1 INTRODUCTION

Quantum electrodynamics is the study of quantized field effects between charged particles via photon interactions. It predicts corrections to relativistic quantum mechanics which have now been tested by a wide variety of high precision experiments. This work is primarily concerned with a study of QED effects in muonic systems. However, we begin with a brief review of the corresponding effects in more familiar electronic systems.

In atomic physics, the principal test of QED is the energy shift of the  $2s_{1/2}$  state relative to the  $2p_{1/2}$  state in hydrogenic ions (the Lamb shift). Lamb and Retherford<sup>1,2,3,4</sup> used radio frequency resonance tuned to the  $2s_{1/2} - 2p_{1/2}$  energy shift to measure the energy difference. This technique has been used more recently in higher precision experiments by Newton et al.<sup>5</sup>, and Lundeen and Pipkin.<sup>6</sup> Quenching anisotropy<sup>7</sup> and laser resonance<sup>8</sup> are two other experimentally used techniques to measure  $2s_{1/2} - 2p_{1/2}$  shifts in higher frequency (higher Z) regions. In the experiments indicated, close agreement with theory was obtained.

In hydrogenic ions the dominant quantum electrodynamic effect in  $2s_{1/2} - 2p_{1/2}$  transitions is the electron self-energy. This effect may be interpreted as the  $2s_{1/2}$  electron interacting with its own radiation field. This interaction

is achieved via the electron emitting a virtual photon and subsequently absorbing it.

The next largest QED effect for electrons is vacuum polarization which corresponds to the creation of virtual electron-positron pairs from the vacuum in the presence of an electric field. These dipole-like pairs surround the nucleus so that the observed charge at a large distance from the nucleus is really a screened charge. Within a shorter range of the nucleus, of the order of the Compton wavelength, the nuclear charge is only partially screened. This produces a small downward shift compared to the much larger upward shift due to the electron self-energy (see 2.10 for a more detailed discussion of orders of magnitude.)

The other major contribution to the  $2s_{1/2} - 2p_{1/2}$  shift is the finite nuclear size. Rather than being a point source, the nuclear charge is distributed over a finite region of space with root mean square radius  $r$ . This produces a further small upward shift of the  $2s_{1/2}$  state.

In addition to QED and finite size effects, the  $2p_{1/2}$  state is shifted upwards by the  $2p_{3/2} - 2p_{1/2}$  fine structure splitting. This is a relativistic, but non-QED effect predicted in lowest order by the Dirac equation.

Thus far only electronic systems have been considered. If the electron in a hydrogenic ion is replaced by a muon, then

vacuum polarization becomes the dominant QED effect. Since the muon is about two hundred times more massive than the electron, the mean nucleus-muon orbital radius is about one two-hundredth of that of the electron. In this region the bare charge is only partially screened and hence the effect due to vacuum polarization is much intensified relative to that of the electron system. Hence, unlike electronic systems, the net QED shift of the  $2s_{1/2}$  state is downward.

Interest in muonic systems has been stimulated by measurements of the  $2s_{1/2} - 2p_{1/2}$  and  $2s_{1/2} - 2p_{3/2}$  energy splittings in the system  $\mu^- \text{He}^{++}$ . Berten et al measured the  $2s_{1/2} - 2p_{3/2}$  energy splitting by using laser resonance in the infrared to stimulate emission at  $8120\text{\AA}$ . Subsequently, Carboni et al<sup>10,11</sup> with higher precision measurements found  $E(2p_{3/2}) - E(2s_{1/2}) = 1527.5 \pm .3\text{meV}$  and  $E(2p_{1/2}) - E(2s_{1/2}) = 1331.3 \pm .5\text{meV}$ . Earlier calculations have been done for hydrogen by Di Giacomo<sup>12</sup> and for Helium by Borie and Rinker<sup>13</sup>. This present work extends these earlier calculations to the  $1s_{1/2}$ ,  $2s_{1/2}$ ,  $2p_{1/2}$ ,  $2p_{3/2}$  energy levels of  $\mu^- \text{Li}^{3+}$  and  $\mu^- \text{Be}^{4+}$ . The lowest order vacuum polarization potential (Uehling potential), and the finite nuclear size are included by direct numerical integration of the Dirac equation for the muonic system.

With the inclusion of the above effects, the  $2s_{1/2} - 2p_{1/2}$

shifts may be determined to leading order. Since the energy splittings nominally scale as  $Z^4$ , one would normally expect the transition frequencies for  $\text{Li}_6$  and  $\text{Be}_9$  to be above the optical region covered by tunable laser sources. However, the present work shows that there is a strong cancellation between the downward vacuum polarization and upward nuclear size shifts. Consequently, some of the predicted transition frequencies lie within the region accessible to experimental measurement.

Further, since the energy shifts are a sensitive function of the nuclear radius, experimental measurements of the shifts would yield improved values for the nuclear radius. On the following page an energy level diagram for  $\text{He}_4^{++} - \mu^-$  illustrates the energy splittings  $2s_{\frac{1}{2}} - 2p_{\frac{1}{2}, \frac{3}{2}}$ .

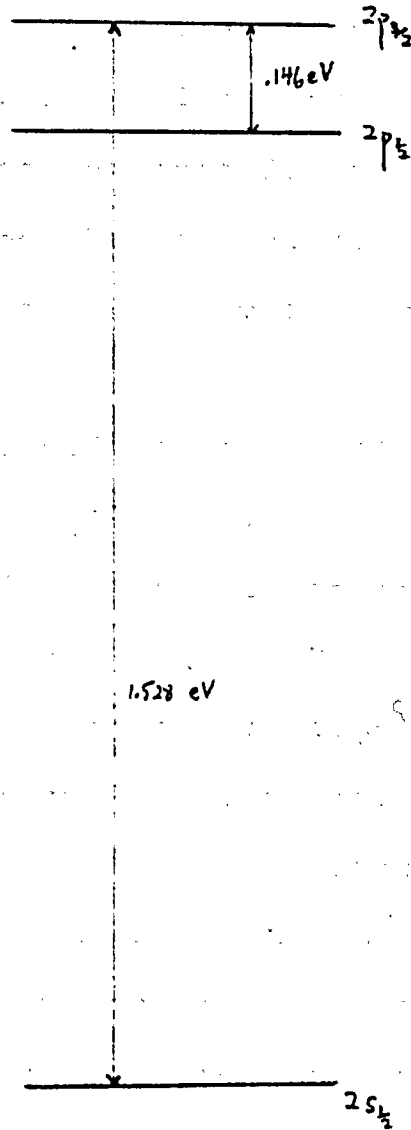


Figure 1.1

ENERGY LEVEL DIAGRAM FOR  $\mu^- \text{He}_4^{++}$

## 2 THEORETICAL DESCRIPTION

In this section the theoretical background useful in the calculation of energy levels for light muon-hydrogenic ions is given. This background consists of the construction of a one-body problem in 2.1, the Dirac equation (2.2) whereby the dominant energies are determined, stationary perturbation calculations (2.3), and the various potentials (2.4-2.7) used in the Dirac equation or stationary perturbation calculations.

The quantum electrodynamic potentials (2.5-2.7) are the  $\alpha Z\alpha$  and  $\alpha Z^2\alpha$  vacuum polarization and the  $\alpha Z\alpha$  muon self-energy. The effect of finite nuclear size corrections to the Coulomb potential is discussed in (2.4).

The  $\alpha Z\alpha$  vacuum polarization potential and the Coulomb potential with finite nuclear size are included in the Dirac equation in order to determine the associated energy levels (see 2.8). The  $\alpha Z\alpha$  vacuum polarization potential and the  $\alpha Z\alpha$  muon self-energy are determined via perturbation theory.

The sum of all the energies are used in determining the total energies of the  $1s_{\frac{1}{2}}, 2s_{\frac{1}{2}}, 2p_{\frac{1}{2}}, 2p_{\frac{3}{2}}$  states and the energy differences  $E(2s_{\frac{1}{2}} - 2p_{\frac{1}{2}, \frac{3}{2}})$ . Those energy differences due to the finite nuclear size Coulomb potential and  $\alpha Z\alpha$  vacuum polarization potential are functions of the nuclear radius. Empirical curve fits are obtained in (3.1).

Finally 2.9 contains leading corrections not included in this work. Their order of magnitude determines the theoretical uncertainty in the predicted energy level splittings.

### 2.1 Centre of mass Motion:

Energy level calculations for two-body systems are simplified if the centre of mass motion can be eliminated. This can be done in the non-relativistic limit by rewriting the total Hamiltonian given by

$$H = \frac{\bar{P}_1^2}{2m_1} + \frac{\bar{P}_2^2}{2m_2} + V(\bar{r}_1 - \bar{r}_2). \quad (2.1.1)$$

in terms of centre of mass and relative coordinates.

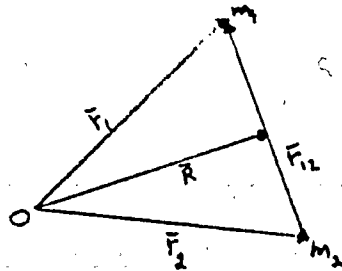


Figure 2.1.1

#### Illustrating Centre of Mass and Relative Coordinates

Referring to figure 2.1.1, the position of the centre of mass is denoted by  $\bar{R}$  where

$$\bar{R} = \frac{m_1 \bar{r}_1 + m_2 \bar{r}_2}{M} \quad (2.1.2)$$

with

$$M = m_1 + m_2. \quad (2.1.3)$$

Using this result with

$$\bar{r}_{12} = \bar{r}_1 - \bar{r}_2 \quad (2.1.4)$$

yields

$$\bar{r}_1 = \bar{R} + \frac{m_2}{M} \bar{r}_{12} \quad (2.1.5)$$

$$\bar{r}_2 = \bar{R} - \frac{m_1}{M} \bar{r}_{12}.$$

Substituting 2.1.5 in 2.1.1 gives

$$\begin{aligned} H &= \frac{m_1}{2} \left[ \frac{d\bar{R}}{dt} + \frac{m_2}{M} \frac{d\bar{r}_{12}}{dt} \right]^2 + \frac{m_2}{2} \left[ \frac{d\bar{R}}{dt} - \frac{m_1}{M} \frac{d\bar{r}_{12}}{dt} \right]^2 + V(\bar{r}_{12}) \\ &= \frac{m_1 + m_2}{2} \left( \frac{d\bar{R}}{dt} \right)^2 + \frac{1}{2M} (m_1 m_2^2 + m_2 m_1^2) \frac{d\bar{r}_{12}}{dt}^2 + V(\bar{r}_{12}) \\ &= \frac{\bar{P}_{cm}^2}{2M} + \frac{\bar{P}_{rel}^2}{2m_r} + V(\bar{r}_{12}) \end{aligned} \quad (2.1.6)$$

where

$$m_r = \frac{m_1 m_2}{M}. \quad (2.1.7)$$

Since the kinetic energy of the centre of mass is a constant of the motion, we can subtract it, leaving

$$H' = \frac{\bar{P}_{rel}^2}{2m_r} + V(\bar{r}_{12}). \quad (2.1.8)$$

Thus the two-body problem has been reduced to an equivalent one-body problem of a particle of reduced mass  $m_r$  orbiting a fixed centre of force.

## 2.2 Dirac Equation:

The Dirac equation is the relativistic analogue of the

single particle Schrodinger equation. It has the form

$$(\vec{\alpha} \cdot \vec{p} + \beta m) \psi = i \frac{\partial \psi}{\partial t} \quad (=E\psi \text{ for stationary states}) \quad (2.2.1)$$

where

$$\psi = \begin{pmatrix} \psi_1 \\ \psi_2 \\ \psi_3 \\ \psi_4 \end{pmatrix} = \begin{pmatrix} \phi \\ \chi \end{pmatrix}, \quad \vec{\alpha} = \begin{pmatrix} 0 & \vec{\sigma} \\ \vec{\sigma} & 0 \end{pmatrix} \quad (2.2.2)$$

in units with  $\hbar=c=1$ . The unit of energy is thus  $mc^2$  a.u. With the introduction of a scalar potential  $\Phi(r)$  in 2.2.1, E becomes

$$E' = E - e\Phi(r) = E - V(r) \quad (2.2.3)$$

and so 2.2.1 is rewritten as

$$[\vec{\alpha} \cdot \vec{p} + \beta m + V(r)] \psi = E \psi. \quad (2.2.4)$$

The total angular momentum operator is given by

$$\vec{J} = \vec{L} + 1/2 \vec{\Sigma} \quad (2.2.5)$$

where

$$\vec{L} = \vec{R} \times \vec{P} \quad \text{and} \quad \vec{\Sigma} = \begin{pmatrix} \vec{\sigma} & 0 \\ 0 & \vec{\sigma} \end{pmatrix} \quad (2.2.6)$$

The eigenvectors of  $\vec{\Sigma}^2$  and  $\Sigma_z$  are

$$K_{\frac{1}{2}} = \begin{pmatrix} 1 \\ 0 \end{pmatrix} \quad \text{and} \quad K_{-\frac{1}{2}} = \begin{pmatrix} 0 \\ 1 \end{pmatrix} \quad (2.2.7)$$

Since  $\vec{J}$  commutes with the Hamiltonian,  $J^2$  and  $J_z$  are constants of the motion. The large component  $\phi$  is an eigenfunction of  $J^2$  and  $J_z$ . It can be constructed by the vector coupling of  $\vec{L}$  and  $\vec{S}$  as follows.

$$\begin{aligned} \phi_{jIM} &= g(r) \sum_{mt} \langle 1, m, 1/2, t | JM \rangle Y_2^m(\hat{r}) K_t \\ &= g(r) \begin{pmatrix} \langle 1, M-1/2, 1/2, 1/2 | JM \rangle Y_2^{M-1/2}(\hat{r}) \\ \langle 1, M+1/2, 1/2, 1/2 | JM \rangle Y_2^{M+1/2}(\hat{r}) \end{pmatrix} \end{aligned} \quad (2.2.8)$$

where the vector coupling coefficients may be obtained from Table (2.2.1). The spherical harmonics  $Y_2^m$  in  $\phi_{jIM}$  are the same as in Akhiezer and Berestetskii but differ by  $(-)^m$  from those in Bethe and Salpeter.

Table 2.2.1

VECTOR COUPLING COEFFICIENTS  $\langle 1, m, 1/2, t | JM \rangle$

t	$1 + \frac{1}{2}$	$1 - \frac{1}{2}$
$\frac{1}{2}$	$\sqrt{\frac{1+M+1/2}{2I+1}}$	$\sqrt{\frac{1-M+1/2}{2I+1}}$
$-\frac{1}{2}$	$\sqrt{\frac{1-M+1/2}{2I+1}}$	$\sqrt{\frac{1+M+1/2}{2I+1}}$

The small component  $\chi_{jIM}$  is related to  $\phi_{jIM}$  through 2.2.1 yielding

$$\chi_{jIM} = \frac{\vec{\sigma} \cdot \vec{p} \phi_{jIM}}{E - V(r) + m_p} \quad (2.2.9)$$

This leads to

$$\chi_{jIM} = if(r) \begin{pmatrix} \langle 1', M-1/2, 1/2, 1/2 | JM \rangle Y_{l'}^{M-1/2}(\hat{r}) \\ \langle 1', M+1/2, 1/2, 1/2 | JM \rangle Y_{l'}^{M+1/2}(\hat{r}) \end{pmatrix} \quad (2.2.10)$$

Substituting 2.2.8 and 2.2.10 into 2.2.4 yields

$$\frac{dg(r)}{dr} + (1+k)\frac{g(r)}{r} = (E - V(r) + m_r)f(r) \quad (2.2.11)$$

$$\frac{df(r)}{dr} + (1-k)\frac{f(r)}{r} = (m_r + V(r) - E)g(r)$$

with

$$k = -(1+1) \quad \text{for } j = 1+1/2, \quad l' = 1+1$$

$$k = 1 \quad \text{for } j = 1-1/2, \quad l' = 1-1. \quad (2.2.12)$$

Setting  $F(r) = rf(r)$ ,  $G(r) = rg(r)$ , 2.2.11 may be rewritten as

$$\frac{dG(r)}{dr} + \frac{kG(r)}{r} = (E - V(r) + m_r)F(r) \quad (2.2.13)$$

$$\frac{dF(r)}{dr} - \frac{kF(r)}{r} = (m_r - E + V(r))G(r).$$

In the numerical integration of the coupled differential equations 2.2.13 it is necessary to have an unnormalized form of  $F(r)$  and  $G(r)$  for  $r$  approaching 0 as a boundary condition. The small  $r$  behaviour may be determined by examining 2.2.13 and considering the leading term of an expansion of  $F(r)$  and  $G(r)$  in powers of  $r$ . For  $k$  greater than zero, as  $r$  approaches zero  $F(r)$  approaches  $r^k$  and  $G(r)$  approaches  $br^{k+1}$ . Using this in 2.2.13 to solve for  $b$  yields:

$$(E - V(0) + m_r)r = b((k+1)+k)r. \quad (2.2.14)$$

Thus

$$b = \frac{E - V(0) + m_p}{2k+1} \quad (2.2.15)$$

For  $k$  less than zero, as  $r$  approaches zero  $G(r)$  approaches  $r^{-k}$  and  $F(r)$  approaches  $Cr^{-k+1}$ . Using this in 2.2.13 gives

$$(V(0) - E + m_p)r^{-k} = C(-k+1-k)r^{-k} \quad (2.2.16)$$

from which:

$$C = \frac{V(0) - E + m_p}{1-2k} \quad (2.2.17)$$

### 2.3 Perturbation Calculations

Non-degenerate perturbation theory is used to calculate the second order correction to the nuclear vacuum polarization. Using standard Rayleigh-Schroedinger perturbation theory, the Hamiltonian is partitioned according to

$$H = H_0 + \lambda V \quad (2.3.1)$$

where

$$H|\psi\rangle = E|\psi\rangle, \quad (2.3.2)$$

$E$  and  $|\psi\rangle$  have the expansions

$$E = E_0 + \lambda E_1 + \lambda^2 E_2 + \dots, \quad (2.3.3)$$

$$|\psi\rangle = |0\rangle + \lambda|1\rangle + \lambda^2|2\rangle + \dots \quad (2.3.4)$$

and

$$H|0\rangle = E|0\rangle. \quad (2.3.5)$$

Substituting  $E$  and  $|\psi\rangle$  into 2.3.2 and equating equal powers of  $\lambda$  leads to

$$E'_l = \lambda E_l = \frac{\langle 0 | V' | 0 \rangle}{\langle 0 | 0 \rangle}, \quad (2.3.6)$$

where  $V' = \lambda V$ .

The Dirac wavefunctions for the scalar potentials are given in the previous section. Using these wavefunctions in 2.3.13 and performing the angular integration yields

$$\begin{aligned} E'_l &= \frac{\int_0^\infty (|f(r)|^2 + |g(r)|^2) V'(r) r^2 dr}{\int_0^\infty (|f(r)|^2 + |g(r)|^2) r^2 dr} \\ &= \frac{\int_0^\infty (|F(r)|^2 + |G(r)|^2) V'(r) dr}{\int_0^\infty (|F(r)|^2 + |G(r)|^2) dr} \end{aligned} \quad (2.3.7)$$

#### 2.4 Finite Nuclear Size

The actual nuclear charge is distributed over a finite region of space instead of being concentrated at a point. A commonly used finite nuclear size model has the nuclear charge density

$$\rho(r) = A e^{-(r/r_0)^2}, \quad (2.4.1)$$

where

$$\int_0^\infty \rho(r) r^2 dr = \alpha^{3/2} Z. \quad (2.4.2)$$

Substituting 2.4.1 in 2.4.2 yields

$$A = \frac{\alpha^{3/2} Z}{\int_0^\infty e^{-(r/r_0)^2} r^2 dr}. \quad (2.4.3)$$

The radial parameter

$$r_0 = (2/3 \langle r^2 \rangle)^{1/2}, \quad (2.4.4)$$

is obtained from

$$\langle r^2 \rangle = \int_0^\infty \rho(r) r^4 dr \quad (2.4.5)$$

In order to evaluate the electrostatic potential for finite nuclear size, apply Gauss's Law. This gives

$$\vec{E} = \frac{\hat{r} \alpha^{1/2} Z \int_0^r e^{-(r'/r_0)^2} r'^2 dr'}{r^2 \int_0^\infty e^{-(r'/r_0)^2} r'^2 dr'} \quad (2.4.6)$$

The corresponding potential is

$$V = -\alpha^{1/2} \int_\infty^r \vec{E} \cdot d\vec{l} = -\alpha Z \frac{\int_0^r \frac{dr'}{r'^2} \int_0^{r'} e^{-u^2} u^2 du}{\int_0^\infty e^{-u^2} u^2 du} \quad (2.4.7)$$

This reduces to

$$V_{E.S.} = -\frac{2\alpha Z}{\sqrt{\pi}} \int_0^{r/r_0} e^{-u^2} du \quad (2.4.8)$$

### 2.5 Leading order Vacuum Polarization

The dominant quantum electrodynamic effect for low Z muonic systems is the  $\alpha^2 \alpha$  vacuum polarization potential. It is illustrated by the Feynman graph shown in Fig 2.5.1.



Figure 2.5.1

$\alpha^2 \alpha$  Vacuum Polarization Potential

In order to evaluate the effect of the closed electron loop, consider the scattering of an electron and a positron as shown in figure 2.5.2 <sup>16</sup>.

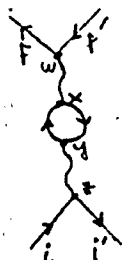


Figure 2.5.2

Electron Positron Scattering in the Field of the  
Leading Order Vacuum Polarization Potential

Using standard techniques of quantum electrodynamics, the scattering matrix is given in the co-ordinate representation by <sup>16</sup>

$$S_{fi} = -(-i \alpha^{1/2})^4 \int d^4w d^4x d^4y d^4z [ \bar{\psi}_F^{(+)}(w) \gamma_\mu \psi_F^{(-)}(w) ] iD_F(w-x) \times \\ \times [ \gamma_\nu^y iS_F(y-x)_{\beta\lambda} \gamma_\tau^\mu iS_F(x-y)_{\tau\kappa} ] iD_F(y-z) \times [ \bar{\psi}_F^{(-)}(z) \gamma_\nu \psi_F^{(+)}(z) ] \quad (2.5.1)$$

where  $D_F$  is the photon propagator and  $S_F$  the electron propagator. In order to evaluate 2.5.1 everything in the integrand is Fourier transformed. The photon propagator is given by

$$D_F(w-x) = \frac{1}{(2\pi)^4} \int d^4q e^{-iq(w-x)} D_F(q^2), \quad (2.5.2)$$

where

$$D_F(q^2) = \frac{-1}{q^2 + i\epsilon}, \quad \epsilon \rightarrow 0^+ \quad (2.5.3)$$

The electron propagator is given in the momentum representation by

$$S_F(p^2) = \frac{1}{\not{p} - m + i\epsilon} \quad (2.5.4)$$

with

$$\not{p} = \gamma^\mu \frac{\partial}{\partial x^\mu} \quad \text{and} \quad \bar{\gamma} = \beta \vec{\alpha}, \quad \gamma^0 = \beta. \quad (2.5.5)$$

After the integrand has been Fourier transformed the coordinate integrals are calculated. Next the momentum space integrals are performed (for this we must cut off high frequency parts and renormalize charge and mass).

Comparing the Scattering Matrix given by figure 2.5.2 with figure 2.5.3 below, a prescription for modifying the photon propagator to obtain higher order corrections is obtained (see figure 2.5.4).



Figure 2.5.3

Electron Positron Scattering via Coulomb Interaction

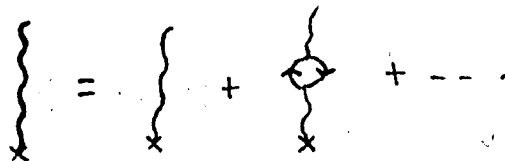


Figure 2.5.4

Expansion of the Exact Photon Propogator

Following Borie and Rinker, the expression for the amplitude of figure 2.5.4 is

$$S_{fi} = U^\dagger(p') U(p) [ + e A_0(\vec{q}) ] (\pm \pi)^3 (\vec{p}' - \vec{p} - \vec{q}), \quad (2.5.6)$$

where the Coulomb gauge  $\nabla \cdot \vec{A} = 0$  is used and

$$\begin{aligned} e A_0(\vec{q}) &= -4\pi Z \alpha \frac{F(\vec{q})}{q^2} \cdot \pm \pi \int (E' - E) \\ &= \int d^3 r V(r) e^{-i\vec{q} \cdot \vec{r}} \pm \pi \int (E' - E). \end{aligned} \quad (2.5.7)$$

Here  $q = (0, \vec{q})$  is a consequence of using the Coulomb gauge.

The nuclear form factor  $F(\vec{q})$  is given by

$$F(\vec{q}) = \int d^3 r \rho(r) e^{-i\vec{q} \cdot \vec{r}}. \quad (2.5.8)$$

The modified photon propagator is written in the form

$$\frac{1}{q^2} \left( 1 + \frac{\Pi(q^2)}{q^2} + \dots \right) \quad (2.5.9)$$

as illustrated in figure 2.5.5. After renormalization the  $\Pi(q^2)/q^2$  correction term is

$$\begin{aligned} \frac{\Pi(q^2)}{q^2} &= \frac{\alpha q^2}{6\pi} \int_1^\infty dz \left( \frac{1}{z^2} + \frac{1}{2z^4} \right) \frac{(z^2 - 1)^k}{z^2 + q^2/4} \\ &= U_2(q). \end{aligned} \quad (2.5.10)$$

Since (2.5.6) results from using  $1/q^2$  for the photon propagator, the above modification for vacuum polarization leads to the leading-order vacuum polarization potential.

$$\begin{aligned} V_{VP1}(q) &= \frac{\Pi(q^2)}{q^2} e A_0(q) \\ &= -4\pi Z \alpha \frac{F(q)}{q^2} U_2(q). \end{aligned} \quad (2.5.11)$$

Fourier transforming (2.5.11) gives

$$V_{VP1}(r) = -\frac{\alpha}{2\pi^2} \int d^3 r' \rho(r') \int d^3 q e^{i\vec{q} \cdot (\vec{r} - \vec{r}')} \frac{U_2(q)}{q^2} \quad (2.5.12)$$

Substituting 2.5.10 for  $U_2(q)$  (with  $\int d^3 q \frac{e^{i\vec{q} \cdot \vec{r}}}{q^2 + 4z^2} = \frac{2\pi^2 e^{-2rz}}{r}$ )

in 2.5.12 yields

$$V_{VP1}(r) = -\frac{2\alpha^2}{3\pi} \int d^3 r' \frac{\rho(r')}{|\vec{r} - \vec{r}'|} X_1(2|\vec{r} - \vec{r}'|) \quad (2.5.13)$$

where

$$X_n(x) = \int_0^\infty dt \frac{(t^2 - 1)^{n/2}}{t^{n+1}} \left[ 1 + \frac{1}{2t^2} \right] e^{-2xt} \quad (2.5.14)$$

By considering a spherically symmetric nuclear charge distribution, the angular integrations of 2.5.13 may be performed leaving

$$V_{VP1}(r) = -\frac{2\alpha^2}{3r} \int_0^\infty dr' r' \rho(r') [X_2(2|r-r'|) - X_2(2|r+r'|)] \quad (2.5.15)$$

To sufficient accuracy, a homogeneous charge distribution,

$$\rho(r) = \begin{cases} \frac{3Z}{4\pi R_N^3} & \text{for } r \leq R \\ 0 & \text{for } r > R \end{cases} \quad (2.5.16)$$

may be used to obtain

$$V_{VP1}(r) = \frac{-2\alpha^2}{2\pi r R_N^3} \left( \frac{2r}{5} + \frac{1}{4} [X_4(2R_N + 2r) - X_4(2R_N - 2r)] \right) + \frac{1}{2} R_N [X_3(2R_N + 2r) - X_3(2R_N - 2r)] \quad (2.5.17a)$$

for  $r$  inside the nuclear radius  $R_N$ . Outside the nuclear radius

$$V_{VPI}(r) = \frac{-z\alpha^2}{2\pi r R_N^3} \left( \frac{1}{4} [X_4(2R_N + 2r) - X_4(2r - 2R_N)] \right. \\ \left. + \frac{1}{2} R_N [X_3(2R_N + 2r) + X_3(2r - 2R_N)] \right). \quad (2.5.17b)$$

The  $X_n(x)$  are given by

$$X_n(x) = E_1(x) \sum_{k \geq \max[0, 1-n]} C_{nk} x^{2k+n-1} + e^{-2r} \sum_{k \geq \min[0, n-1]} D_{nk} x^k \quad (2.5.18)$$

where

$$E_1(x) = \int_1^\infty dt \frac{e^{-xt}}{t} \quad (2.5.19)$$

and the  $C_{nk}$ 's and  $D_{nk}$ 's can be evaluated from recurrence relations given by Huang. Alternately a power series expansion for  $V_{VPI}(r)$  may be obtained. This is accomplished by first rewriting 2.5.15 and using 2.5.16 yielding

$$V_{VPI}(r) = \frac{-\alpha^2 z}{2\pi r R_N^3} \int_0^{R_N} dr' r' [K_0(2|r-r'|) - K_0(2|r+r'|)] \quad (2.5.20)$$

where

$$K_0(x) = - \int_1^\infty dt e^{-xt} \left( \frac{1}{t^3} + \frac{1}{2t^5} \right) (t^2 - 1)^{1/2} \quad (2.5.21)$$

and

$$K_0(x) = (-)^n \frac{d^n}{dx^n} K_0(x). \quad (2.5.22)$$

A Taylor expansion of the  $K_n$ 's in 2.5.20 is then performed about  $2r$  to yield a useful expression for  $V_{VPI}(r)$  for  $r$

reasonably larger than the nuclear radius. Thus

$$K_0(2(r+r')) = K_0(2r) + K_0'(2r)(2r') + \dots \quad (2.5.23)$$

so that

$$K_0(2(r+r')) - K_0(2(r-r')) = 2[K_0(2r)2r' + \frac{K_3(2r)(2r')^3}{3!} + \frac{K_5(2r)(2r')^5}{5!} + \dots] \quad (2.5.24)$$

is used in (2.5.20). Integration gives

$$V_{VP1}(r) = -2\alpha^2 2[K_1(2r) + \frac{2R_N^2}{5}K_3(2r) + \frac{2R_N^4}{35}K_5(2r) + \dots] \quad (2.5.25)$$

Fullerton and Rinker expand  $K_n(x)$  for  $x$  in  $[1, \infty)$  as

$$K_n(x) = \frac{e^{-x} \sum_{i=1}^N d_i x^{-i}}{x^{3/2} \sum_{k=1}^S e_k x^{-k}} \quad (2.5.26)$$

The coefficients  $d_i, e_k$  are listed by them. The computational ease of 2.5.26 for  $x$  in  $[1, \infty)$  makes it preferable to (2.5.17).

The nuclear radius  $R_N$  for the homogeneous charge distribution 2.5.16 is related to the root mean square (RMS) radius by

$$\begin{aligned} \sqrt{\langle r^2 \rangle} &= \frac{\int_0^{R_N} \rho(r) r^4 dr}{\int_0^{R_N} \rho(r) r^2 dr} \\ &= \sqrt{3/5} R_N. \end{aligned} \quad (2.5.27)$$

2.6. ( $\alpha^2 \propto \alpha$ ) Vacuum Polarization Potential:

The second order vacuum polarization contributions are illustrated in the Feynman graphs of figure 2.6.1.

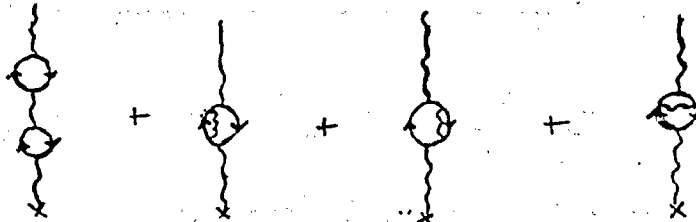


Figure 2.6.1

$\alpha^2 \propto \alpha$  Vacuum Polarization Potential

Following the same type of procedure as outlined in the previous section, Kallen and Sabry obtained <sup>13</sup>

$$V_{VP2}(\bar{q}) = -4\pi Z\alpha \frac{F(\bar{q})}{\bar{q}^2} U_4(q) \quad (2.6.1)$$

where  $U_4(q)$  is given in reference 13. Blomqvist gave the following useful expression for  $V_{VP2}(r)$  as <sup>18</sup>

$$V_{VP2}(r) = \frac{-Z\alpha R_{21}(r)}{r} \quad (2.6.2)$$

where

$$R_{21}(r) = -\frac{\alpha^2}{\pi^2} \int_1^\infty dt e^{-2tr} \left\{ \left( \frac{13}{54t^2} + \frac{7}{108t^4} + \frac{2}{9t^6} \right) (t^2 - 1)^{\frac{1}{2}} \right. \\ + \left( \frac{-44}{9t} + \frac{2}{3t^3} + \frac{5}{4t^5} + \frac{2}{9t^7} \right) \cdot \ln[t + (t^2 - 1)^{\frac{1}{2}}] \\ + \left( \frac{4}{3t^2} + \frac{2}{3t^4} \right) (t^2 - 1)^{\frac{1}{2}} \ln[3t(t^2 - 1)] \\ \left. + \left( \frac{-8}{3t} + \frac{2}{3t^3} \right) \int_t^\infty dx f(x) \right\} \quad (2.6.3)$$

and

$$f(x) = \frac{3x^2-1}{x(x^2-1)} \ln[x+(x^2-1)] - \frac{1}{(x^2-1)^2} \ln[8x(x^2-1)] \quad (2.6.4)$$

The small  $r$  expansion is given by<sup>21</sup>

$$\begin{aligned} V_{\nu p 2}(r) = & \frac{\alpha^2 Z^2}{\pi^2} \left( \frac{-4}{9r} (\ln r + C)^2 - \frac{13}{54r} (\ln r + C) - \frac{1}{r} [Z(3) + \frac{\pi^2}{27} + \frac{65}{648}] \right. \\ & + \frac{13\pi^2}{9} + \frac{32\pi \ln 2}{9} - \frac{766\pi}{135} + \frac{5r(\ln r + C)}{3} - \frac{65r}{18} \\ & + \left( \frac{14\pi^2}{27} - \frac{80\pi}{81} \right) r^2 - \frac{5}{18} r^3 (\ln r + C)^2 + \frac{323r^3}{216} (\ln r + C) \\ & \left. + \left( \frac{1}{6} Z(3) - \frac{5\pi^2}{216} - \frac{6509}{2592} \right) r^3 + O(r^4) \right) \quad (2.6.5) \end{aligned}$$

where  $Z(x)$  is the Riemann-zeta function and  $C$  is Euler's constant.

## 2.7 Muon Self Energy:

The muon self energy of order  $\alpha^2$  is the next leading quantum electrodynamic effect as illustrated in figure 2.7.1.



Figure 2.7.1

$\alpha^2$  Muon Self Energy

Using lower order scattering amplitudes and comparing them

with higher order scattering amplitudes, the muon propagator is modified according to figure 2.7.2.

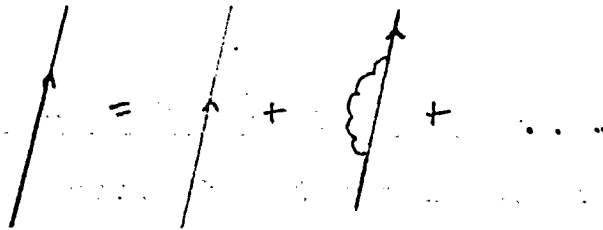


Figure 2.7.2

Expansion of the Exact Muon Propagator

After cancelling the divergences on the right side of figure 2.7.2 and renormalizing the fermion mass, the potential for the self-energy may be determined. A perturbation calculation for the muon self-energy including higher order corrections yields

$$E_{S.E.} = \frac{-\alpha(\infty)^4}{6\pi} m^2 \left[ (1+m^2)^{-3} \left( \frac{19}{30} + \ln(\infty)^{-2} - \ln \frac{\epsilon_{20}}{\epsilon_{21}} \right) - (1+m^2)^{-2} \frac{C_{1j}}{8} + 3\pi\alpha \frac{2(139 - \frac{1}{2} \ln 2)}{128} \right] \quad (2.7.1)$$

Here  $\ln \frac{\epsilon_{20}}{\epsilon_{21}}$  is calculated from the Bethe logarithms giving

$$\ln \frac{\epsilon_{20}}{\epsilon_{21}} = \ln \left( \frac{\epsilon_{20}}{Z^2 R_\infty} \right) - \ln \left( \frac{\epsilon_{21}}{Z^2 R_\infty} \right) \approx 2.81177 + .03002 = 2.84179. \quad (2.7.2)$$

$C_{1j}$  is defined by

$$C_{1j} = \begin{cases} \frac{1}{1+1} & \text{for } j = 1 + 1/2 \\ -\frac{1}{1} & \text{for } j = 1 - 1/2, \end{cases} \quad (2.7.3)$$

and  $m'$  is the muon mass,  $M$  the nuclear mass. ...

### 2.8 Calculation of Energy Levels:

A method must be devised to calculate the Dirac eigenvalues with the potential energies used in 2.2.2. Our numerical integration method involves evaluating the scaled large and small components,  $G(r)$  and  $F(r)$  respectively, at large values of  $r$  for a variety of energy ( $E$ ) values. Since the norm

$$\langle \psi | \psi \rangle = \int_0^{\infty} (|F(r)|^2 + |G(r)|^2) dr \quad (2.8.1)$$

must be finite for eigenfunctions,  $|F(r)|$  and  $|G(r)|$  must approach zero as  $r$  becomes large. On the other hand, for energies not equal to eigenvalues,  $|F(r)|$  and  $|G(r)|$  diverge exponentially. This leads to a prescription for finding the energy levels of 2.2.13. The energy levels are varied so as to minimize  $|F(r)|$  and  $|G(r)|$  at large  $r$ .

This method was used for the Dirac equation containing the sum of the finite nuclear size 2.4.8 and the leading order vacuum polarization potentials (2.5.17,25) to determine the bound state energies  $1s_{\frac{1}{2}}$ ,  $2s_{\frac{1}{2}}$ ,  $2p_{\frac{1}{2}}$ ,  $2p_{\frac{3}{2}}$ . In particular for  $Be_9$ ,  $F(r)$  and  $G(r)$  for these bound state energies are plotted in section 3.1

The calculation of the energy correction due to the

$\alpha^2 Z\alpha$  vacuum polarization term was done using the stationary perturbation result 2.3.7. The wavefunctions that are obtained by solving 2.2.13 for the finite nuclear size and the leading order vacuum polarization potentials included are used, and the  $\alpha^2 Z\alpha$  potential correction 2.6.2 is regarded as the perturbation.

### 2.9 Other Corrections:

The largest correction unaccounted for by this work is that of nuclear polarization. This accounts in  $\mu\text{-He}_4^{++}$  for about .2% of  $E(2s_{1/2} - 2p_{1/2,3/2})$ . In order to estimate how the nuclear polarization correction to the energy levels scales with nuclear charge, consider the nucleus as being made up of  $Z$  positive charges

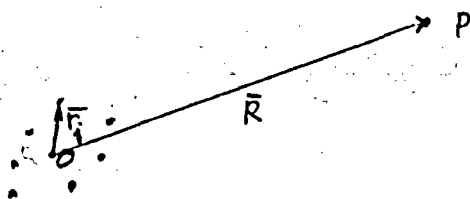


Figure 2.9.1

Observation Point P Outside a Discrete  
Nuclear Charge Distribution

The interaction with an orbiting electron is then given by

$$\begin{aligned}
 V &= \sum_{j=1}^Z \frac{\alpha}{|\vec{R} - \vec{r}_j|} = \alpha \sum_{j=1}^Z \sum_{\ell=0}^{\infty} \frac{r_j^{\ell}}{R^{\ell+1}} P_{\ell}(\cos \theta_j) \\
 &= \left( \frac{1}{R} + \frac{r \cos \theta_j}{R^2} + \dots \right). \tag{2.9.1}
 \end{aligned}$$

For  $r < R$  so that asymptotically,

$$V \approx \frac{\alpha Z}{R} + V_D \tag{2.9.2}$$

where

$$V_D = \frac{\alpha r_j \cos \theta_j}{R^2}. \tag{2.9.3}$$

The first term in (2.9.2) is simply the nuclear ground state Coulomb interaction and the second term,  $V_D$ , may be considered a perturbation. A first order perturbation calculation for the ground state of the nucleus gives no contribution because  $V_D$  is of odd parity. Therefore second order perturbation theory must be used. This gives

$$\begin{aligned}
 \Delta E_{N.P.} &\approx \sum_n \frac{\langle 1 | V_D | n \rangle \langle n | V_D | 1 \rangle}{E_n - E_1} \\
 &= \frac{1}{R^4} \frac{|\langle 1 | r_j \cos \theta_j | n \rangle|^2}{E_n - E_1} \\
 &\approx \frac{\alpha_D}{R^4} \tag{2.9.4}
 \end{aligned}$$

where  $|1\rangle$  is the nuclear ground state. Since  $R$  scales as  $1/2$

$$\Delta E_{N.P.} \approx \alpha_D' \tag{2.9.5}$$

where  $\alpha_D'$  is the model dependent nuclear polarizability. Its value can in principal be determined from nuclear scattering data. Since the leading order corrections to the  $2s_{1/2} - 2p_{1/2}$  energy splittings scale  $\sim Z^4$  (see 2.10), the order of

magnitude of the relative uncertainty in the energy splittings to the nuclear polarization correction should remain constant in all of the above considered.

Next, the muon vacuum polarization accounts for about 0.022% of the energy splittings  $E(2s_{k, \frac{1}{2}} - 2p_{k, \frac{1}{2}})$  for  $\text{He}_4^{++} - \mu^-$ . Other corrections are vertex corrections of order  $\alpha(Z\alpha)^n$  for  $n$  greater than 2 and  $\alpha^2\alpha$  corrections contributing about 0.013% in  $E(2s_{k, \frac{1}{2}} - 2p_{k, \frac{1}{2}})$  for  $\mu^- - \text{He}_4^{++}$ . Breit recoil and two photon interactions account for about 0.01% in  $E(2s_{k, \frac{1}{2}} - 2p_{k, \frac{1}{2}})$  of  $\mu^- - \text{He}_4^{++}$ .

The relativistic corrections to the elimination of the centre of mass motion (Section 2.1) becomes relatively less important with increasing  $Z$ , since the nuclear mass increases roughly in proportion to twice the atomic number (for stable nuclei). The two body problem approaches that of a muon moving in the field of an infinitely heavy nucleus.

### 2.10 Orders of Magnitude

Q.E.D. potentials are identified as terms in expansions of Feynman diagrams. The dependence of each diagram on  $Z$  and  $\alpha$  is determined through the calculation of its scattering amplitude. The Coulomb potential of order  $\alpha Z$  is shown in figure 2.10.1.

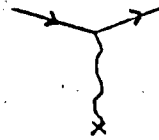


Figure 2.10.1

Muon Scattering via the Coulomb Interaction

The vacuum polarization potentials involve modifying the photon propagator (see Figures 2.5.1 and 2.6.1) by introducing pairs of vertices, each pair contributing  $\alpha$ . The first order vacuum polarization potential is then seen to be of order  $\alpha^2 Z \alpha$  while the second order vacuum polarization is of order  $\alpha^3 Z \alpha$ .

The leading order muon self energy potential (Figure 2.7.1) contains a pair of vertices giving a factor of  $\alpha$ . The scattering process is also the result of the Coulomb interaction of order  $\alpha Z$ . The complete scaling is given by  $\alpha^2 Z \alpha$ .

It is useful to consider the order of magnitude of various corrections through nonrelativistic perturbation calculations. Since the  $2s_{1/2}$  -  $2p_{1/2}$  energy differences are being considered, the wavefunctions for  $2s$  and  $2p$  states are required. These are given by

$$\begin{aligned} \psi(2s) &= (2m_r \alpha)^{3/2} \frac{1}{2\sqrt{2}} (2 - 2m_r \alpha r) e^{-2m_r \alpha r/2} \\ \psi(2p) &= (2m_r \alpha)^{3/2} \frac{1}{2\sqrt{6}} 2m_r \alpha r e^{-2m_r \alpha r/2} \end{aligned} \tag{2.10.1}$$

and the perturbation calculation is given by

$$\Delta E = \int (|\psi(2s)|^2 - |\psi(2p)|^2) \Delta V r^2 dr. \quad (2.10.2)$$

Using the point nucleus leading order vacuum polarization given by

$$V_{VP1} = -\frac{2Z\kappa^2}{3\pi r} \int_0^\infty e^{-2rt} \left(1 + \frac{1}{2t^2}\right) \frac{(t^2-1)^{1/2}}{t^2} dt, \quad (2.10.3)$$

in (2.10.2) gives

$$\Delta E_{VP1} = -\frac{\alpha^5 Z^4 m_r^3}{12\pi} \int_0^1 \frac{(1+z^2/2)(1-z^2)^{1/2}}{(1+\beta z)^4} z dz. \quad (2.10.4)$$

The muon self energy can be viewed as a correction to the interaction energy with the Coulomb field given by

$$\langle \delta V \rangle = \langle V(r+\delta r) - V(r) \rangle \approx \frac{1}{6} (\delta r)^2 \langle \nabla^2 V \rangle \quad (2.10.5)$$

where

$$(\delta r)^2 \approx \langle (\delta r)^2 \rangle = (2\alpha^3 a^2 / \pi) \ln(\alpha Z)^{-1} \quad (2.10.6)$$

and

$$\nabla^2 V = 4\pi Z\alpha \delta^3(r) \quad (2.10.7)$$

Substituting 2.10.7 and 2.10.6 in 2.10.5 and using  $\frac{\psi(2s)}{\sqrt{4\pi}}$  from 2.10.1 gives

$$\Delta E_{SE} = \frac{\alpha^5 Z^4}{3\pi} m_r \ln(\alpha Z)^{-1} \quad (2.10.8)$$

In order to determine the order of magnitude of the finite size correction to the point Coulomb case consider a homogeneous uniformly charged sphere of radius R. Applying Gauss's Law inside the sphere gives

$$E = \frac{rZe}{R^3} \quad (2.10.9)$$

The potential is then given by

$$\begin{aligned}
 V_{\text{F.S.}} &= -\frac{\alpha E}{R} + \frac{\alpha E}{R} \int_R^r r' dr' = \frac{\alpha E}{2R} \left( \frac{r^2}{R^2} - 3 \right) \quad r < R \\
 &= -\frac{\alpha E}{r} \quad r > R
 \end{aligned}
 \tag{2.10.10}$$

Noting the deviation of this result from the point Coulomb case gives

$$\begin{aligned}
 \Delta V_{\text{F.S.}} &= -\frac{\alpha E}{r} + \frac{\alpha E}{2R} \left[ \frac{r^2}{R^2} - 3 \right] \quad r < R \\
 &= 0 \quad r > R,
 \end{aligned}
 \tag{2.10.11}$$

Next a perturbation calculation is used. Noting that for small  $r$   $\psi_{2p}(r) \approx 0$  and  $\psi_{2s}(r)$  approaches a constant (see 2.10.1) the correction due to finite nuclear size is then

$$\begin{aligned}
 \langle \Delta V_{\text{F.S.}} \rangle &\approx |\psi_{2s}(0)|^2 \int_0^R \left( \frac{\alpha E}{r} + \frac{\alpha E}{2R} \left[ \frac{r^2}{R^2} - 3 \right] \right) r^2 dr \\
 &= \frac{E^4 \alpha R^2}{3^3 20} = \frac{\alpha^4 E^4 m_r^3 R^2}{20}
 \end{aligned}
 \tag{2.10.12}$$

Using (2.5.27) gives

$$\langle \Delta V_{\text{F.S.}} \rangle \approx \frac{\alpha^4 E^4 m_r^3}{12} \langle r^2 \rangle.
 \tag{2.10.13}$$

### 3 RESULTS

In this section, the muon energy level and energy difference calculations are tabulated. Table 3.1.1 gives the energy levels for the muon systems obtained as a solution of the Dirac equation with the finite nuclear size and leading order vacuum polarization potentials. Table 3.1.2 has the  $2s_{\frac{1}{2}}$  -  $2p_{\frac{1}{2}}$  energy splittings obtained from Table 3.1.1. Table 3.1.2 also gives the nuclear radial dependance of the energy splittings. Tables 3.1.3 and 3.1.4 give corrections due to the  $\alpha^2 Z \alpha$  vacuum polarization and  $\alpha^2 \kappa$  muon self energy potentials respectively. In Table 3.1.5 the total energy splittings and their associated wavelengths are tabulated. Table 3.1.6 contains the  $2p_{\frac{3}{2}}$  -  $2p_{\frac{1}{2}}$  energy difference due primarily to fine structure. The subscripts of entries in these tables indicate the magnitude of uncertainty in the final figure quoted. Table 3.1.7 summarizes the methods used to obtain these uncertainties.

Graphs 1-8 show the wave functions obtained by numerical integration of 2.2.13 in the following order:  $1s_{\frac{1}{2}}$  G(r),  $1s_{\frac{1}{2}}$  F(r),  $2s_{\frac{1}{2}}$  G(r),  $2s_{\frac{1}{2}}$  F(r),  $2p_{\frac{1}{2}}$  G(r),  $2p_{\frac{1}{2}}$  F(r),  $2p_{\frac{3}{2}}$  G(r),  $2p_{\frac{3}{2}}$  F(r). The wavefunctions are unnormalized and magnified by an appropriate power of ten, with r in relativistic length units ( $\alpha a_0 = 1$ ). The normalization factors needed for the perturbation calculations are indicated on graphs 3 and 5 as A where

$$A^2 \int_0^\infty (|F|^2 + |G|^2) dr = 1, \quad (3.1.1)$$

Section 3.2 outlines the computational procedures used in the determination of the results, linked with a discussion of the uncertainties involved. Finally section 3.3 gives a discussion of the results. In all of the following tables r.E.u. is a relativistic energy unit ( $\frac{1}{2}$  atomic units).

Constants

The following are the values of the constants used.

$$\alpha = 1/137.03608$$

	H <sub>1</sub>	H <sub>2</sub>	He <sub>4</sub>	Li <sub>6</sub>	Be <sub>9</sub>
$\mu$	185.841	195.741	201.069	202.941	204.198

TABLE B.1.1

DIRAC ENERGY EIGENVALUES OBTAINED WITH  $\alpha^2\alpha$  VACUUM  
 POLARIZATION AND FINITE SIZE COULOMB POTENTIALS  
 (in units of  $10^{-13}$  r.E.U.)

$R(10^{-13} \text{ cm})$	$E(1s_{\frac{1}{2}})$	$E(2s_{\frac{1}{2}})$	$E(2p_{\frac{1}{2}})$	$E(2p_{\frac{3}{2}})$
.832	-.495186968,	-.123747861,		
H <sub>1</sub> .862	-.495186555,	-.123747809,	-.123708413,	-.123706766,
.892	-.495186128,	-.123747756,		
2.0	-.52156061,	-.130339063,		
H <sub>2</sub> 2.1	-.52155676,	-.130338582,	-.130299198,	-.130297462,
2.2	-.52155273,	-.130338079,		
1.643	-2.1447953,	-.53574705,		
H <sub>2,4</sub> 1.673	-2.1447793,	-.53574505,	-.53547555,	-.53544699,
1.703	-2.1447630,	-.53574301,		
2.46	-4.8706291,	-1.21665263,	-1.21636242,	-1.21621636,
Li <sub>2</sub> 2.56	-4.8702259,	-1.21660228,	-1.21636242,	-1.21621636,
2.66	-4.8698080,	-1.21655010,	-1.21636242,	-1.21621635,
2.42	-8.7122312,	-2.17643029,	-2.17653303,	-2.17606817,
Be <sub>q</sub> 2.52	-8.7109840,	-2.17627451,	-2.17653301,	-2.17606851,
2.62	-8.7096922,	-2.17611310,	-2.17653330,	-2.17606866,

TABLE 3.1.2

$2s_{1/2} - 2p_{1/2}$  ENERGY DIFFERENCES OBTAINED WITH  $\alpha \approx$  VACUUM POLARIZATION AND FINITE SIZE COULOMB POTENTIALS

(in units of  $10^{-6}$  r.E.u.)

$R_N (10^{-13} \text{ cm})$	$E(2s_{1/2} - 2p_{1/2})$	$E(2s_{1/2} - 2p_{3/2})$
.832	-.39448	-.41095
.862	-.39396	-.41043
.892	-.39343	-.40990
$-.402643 + .0147514R_N^2 - .355661 \times 10^{-2} R_N^3$	$-.355661 \times 10^{-2} R_N^3$	$-.419113 + .0147514R_N^2 - .355661 \times 10^{-2} R_N^3$
2.0	-.39865	-.41601
2.1	-.39384	-.41120
2.2	-.38881	-.40617
$.446553 + .0124297R_N^2 - .226929 \times 10^{-3} R_N^3$	$-.226929 \times 10^{-3} R_N^3$	$-.463913 + .0124297R_N^2 - .226929 \times 10^{-3} R_N^3$
1.643	-2.7150	-3.0006
1.673	-2.6950	-2.9806
1.703	-2.6746	-2.9602
$-3.23864 + .180224R_N^2 + .837181 \times 10^{-2} R_N^3$	$.837181 \times 10^{-2} R_N^3$	$-3.52424 + .180224R_N^2 + .837181 \times 10^{-2} R_N^3$
2.46	-2.9021	-4.3627
2.56	-2.3986	-3.8592
2.66	-1.8762	-3.3374
$-9.14937 + 1.08763R_N^2 - .0224777R_N^3$	$-.0224777R_N^3$	$-10.61 + 1.08763R_N^2 - .0224777R_N^3$
2.42	+1.0274	-3.6212
2.52	+2.5850	-2.0600
2.62	+4.2020	-.4364
$-17.7955 + 3.32699R_N^2 - .047486R_N^3$	$-.047486R_N^3$	$-22.2081 + 3.19909R_N^2 - .0104614R_N^3$

TABLE 3.1.3

PERTURBATION CALCULATIONS OF THE  $\alpha^{2Z\alpha}$  VACUUM  
POLARIZATION CORRECTION

(in units of  $10^{-9}$  r.E.u.)

	$E(2s_{1/2})$	$E(2p_{1/2})$	$E(2s_{1/2} - 2p_{1/2})$
H <sub>1</sub>	-3.235 <sub>2</sub>	-.2843 <sub>2</sub>	-2.951 <sub>4</sub>
H <sub>2</sub>	-3.601 <sub>2</sub>	-.3426 <sub>2</sub>	-3.258 <sub>4</sub>
He <sub>4</sub>	-29.79 <sub>2</sub>	-7.177 <sub>2</sub>	-22.61 <sub>4</sub>
Li <sub>6</sub>	97.28 <sub>2</sub>	-34.12 <sub>2</sub>	-63.16 <sub>4</sub>
Be <sub>9</sub>	222.8 <sub>2</sub>	-95.15 <sub>2</sub>	-127.7 <sub>4</sub>

TABLE 3.1.4

PERTURBATION CALCULATIONS OF THE MUON  
SELF-ENERGY CORRECTION

(in units of  $10^{-9}$  r.E.u.)

	$E(2s_{1/2} - 2p_{1/2})$	$E(2s_{1/2} - 2p_{3/2})$
H <sub>1</sub>	1.292	1.258
H <sub>2</sub>	1.507	1.469
He <sub>4</sub>	21.66	21.01
Li <sub>6</sub>	99.5	96.18
Be <sub>9</sub>	290.9	280.3

TABLE 3.1.5

TOTAL  $E(2s_{1/2} - 2p_{1/2, 3/2})$  ENERGY SPLITTINGS AND THEIR ASSOCIATED WAVELENGTHS

	$E(2s_{1/2} - 2p_{1/2})$	(Å)	$E(2s_{1/2} - 2p_{3/2})$	(Å)
H <sub>1</sub>	$-3.9562 \times 10^{-7}$ ( $-0.20217\text{eV}$ )	61329	$-41212 \times 10^{-7}$ ( $-2.1060\text{eV}$ )	58874
H <sub>2</sub>	$-3.9559 \times 10^{-7}$ ( $-0.20215\text{eV}$ )	61334	$-4.1299 \times 10^{-7}$ ( $-0.21104\text{eV}$ )	58750
He <sub>4</sub>	$-2.6960 \times 10^{-6}$ ( $-1.3777\text{eV}$ )	8999.7	$-2.9822 \times 10^{-6}$ ( $-1.5239\text{eV}$ )	81360
Li <sub>6</sub>	$-2.3623 \times 10^{-6}$ ( $-1.2072\text{eV}$ )	10271	$-3.8262 \times 10^{-6}$ ( $-1.9552\text{eV}$ )	6341.3
Be <sub>9</sub>	$2.7482 \times 10^{-6}$ ( $1.4044\text{eV}$ )	8828.7	$-1.9074 \times 10^{-6}$ ( $-0.97470\text{eV}$ )	12720

TABLE 3.1.6

$E(2p_{3/2}) - E(2p_{1/2})$  ENERGY DIFFERENCES

(Primarily Fine structure)

	r.E.u.	(eV)
H <sub>1</sub>	$1.650 \times 10^{-9}$	$(8.431 \times 10^{-3})$
H <sub>2</sub>	$1.740 \times 10^{-8}$	$(8.891 \times 10^{-3})$
He <sub>4</sub>	$2.862 \times 10^{-7}$	$(1.462 \times 10^{-1})$
Li <sub>6</sub>	$1.464 \times 10^{-6}$	$(7.481 \times 10^{-1})$
Be <sub>9</sub>	$4.656 \times 10^{-6}$	(2.379)

TABLE 3.1.7

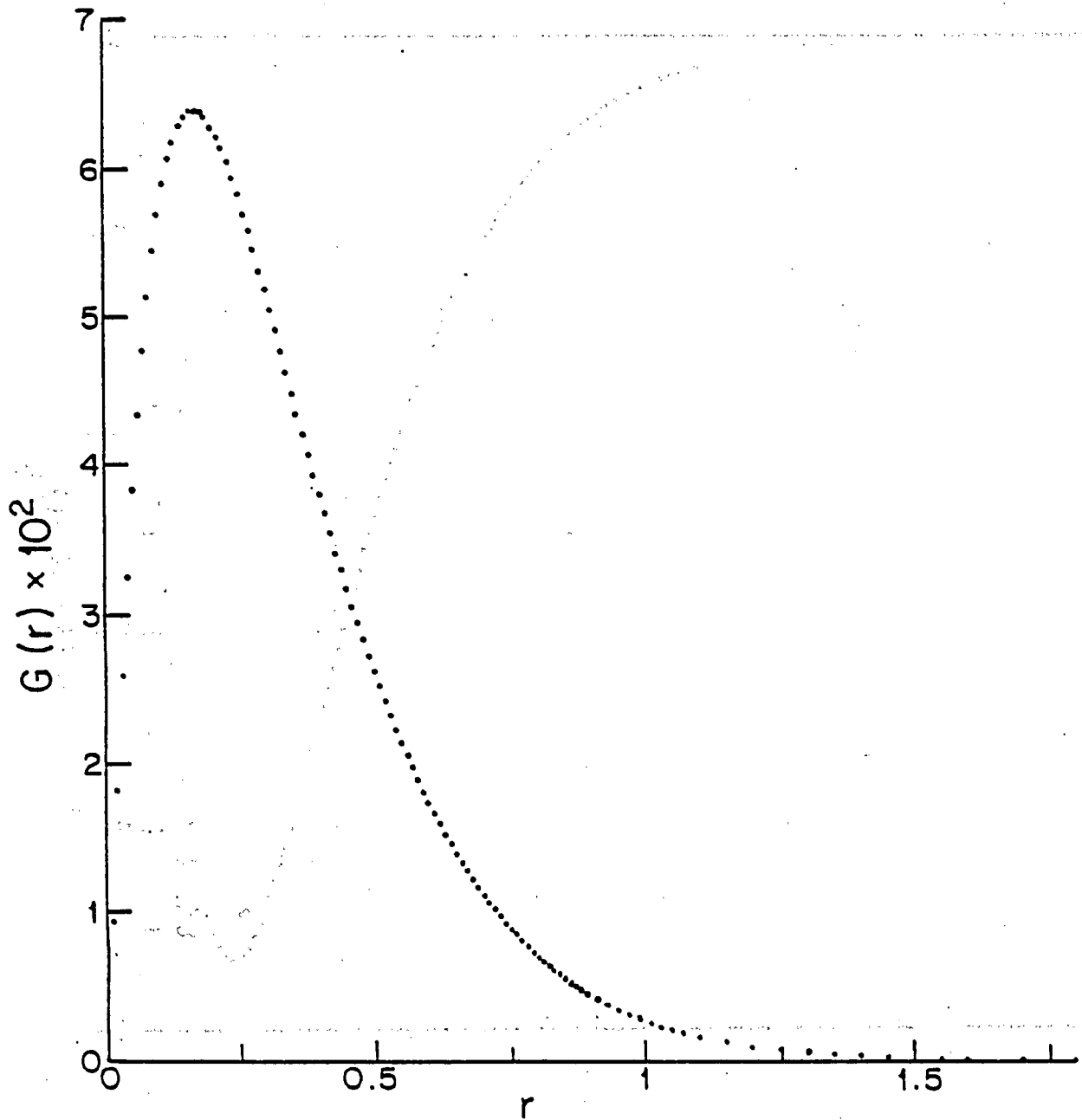
METHODS USED IN THE DETERMINATION OF UNCERTAINTIES

Source	Method	Uncertainty
$U_{\alpha^2\alpha}$ V.P.	Uncertainties in the expansions used were checked by comparing with numerical integration.	$\sim 2\%$ in the fifth figure.
$E_{\alpha^2\alpha}$ V.P. & Finite Size	1) Varying the accuracy level of the numerical integration. 2) Varying the distance to the point of observation (see 3.2) 3) Comparison with known results for $H_1$ and $He_4$ .	See Table 3.1.1
$V_{\alpha^2\alpha}$ V.P.	1) Accuracy of small $r$ expansions known. 2) Accuracy of course curve fits estimated by comparison with values computed through numerical integration.	1) $\sim 1\%$ in the third figure. 2) $\sim 3\%$ $1.5 < r < 2.5$ $\sim 6\%$ $2.5 < r < 3.5$
$\Delta E_{\alpha^2\alpha}$ V.P.	1) Varying the accuracy of the numerical integration. 2) Varying the upper limit cutoff (see 3.2) for the perturbation calculation. 3) Comparison with known results for $He_4$ and $H_1$ .	See Table 3.1.3
Correction for not using a Gaussian charge distribution in the $E_{\alpha^2\alpha}$ V.P.	Estimated by varying the nuclear radius by 10% and noting the difference in energy splittings.	$Li_2$ : $\sim 3\%$ in the fourth figure. $Be_9$ : $\sim 1\%$ in the third figure

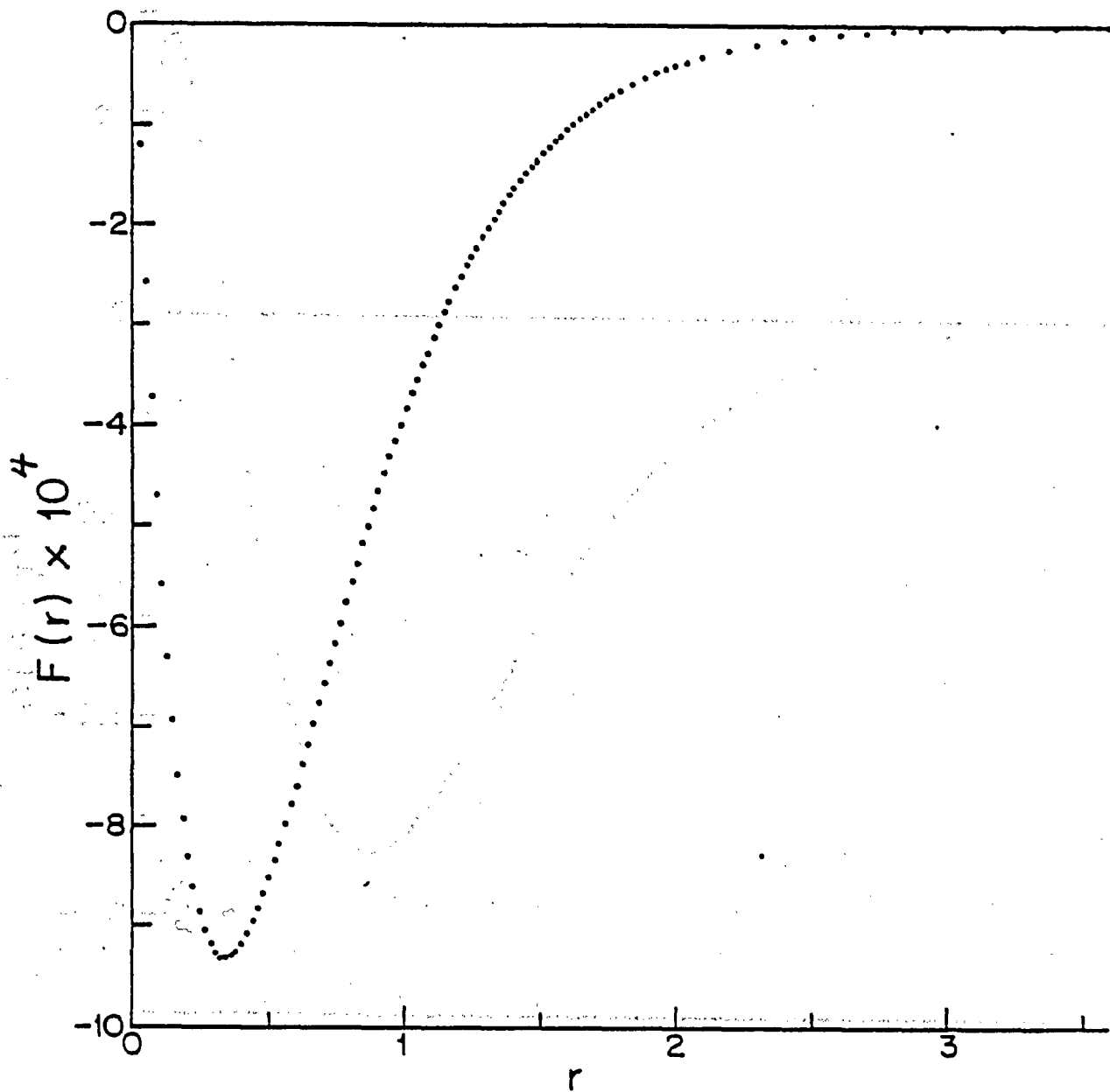
Table 3.1.7 (continued)

Source	Methods	Uncertainties
$\Delta E$ ( $2s_{1/2} - 2p_{1/2}, 3/2$ ) curve fits	Estimated by comparing values of calculated splittings with curve fits.	See 3.2
Nuclear Polarization	See 2.9	

$Be_9 1s_{1/2}$  Unnormalized  $G(r)$  vs  $r$

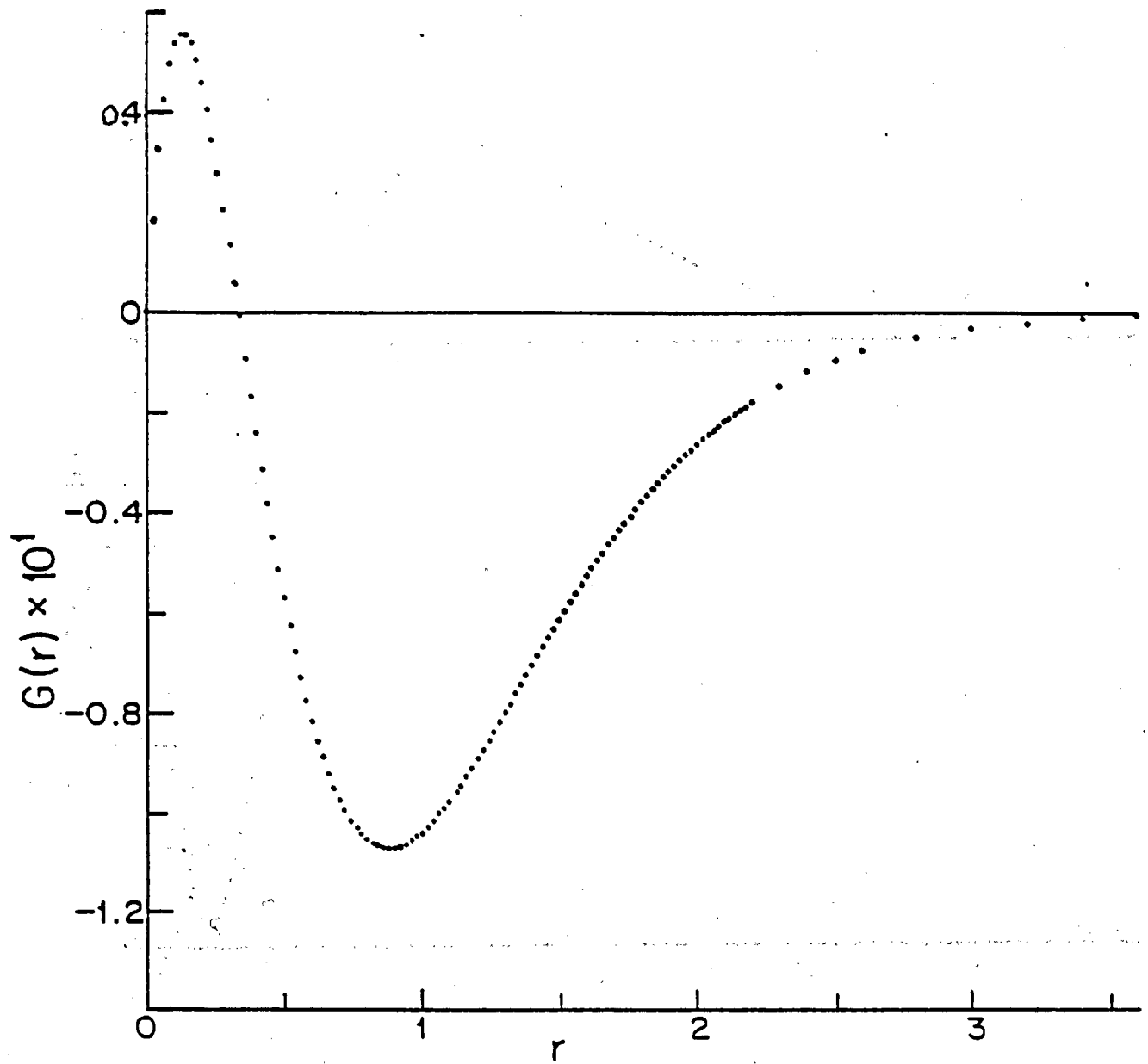


Req 1s<sub>1/2</sub> Unnormalized F(r) vs r

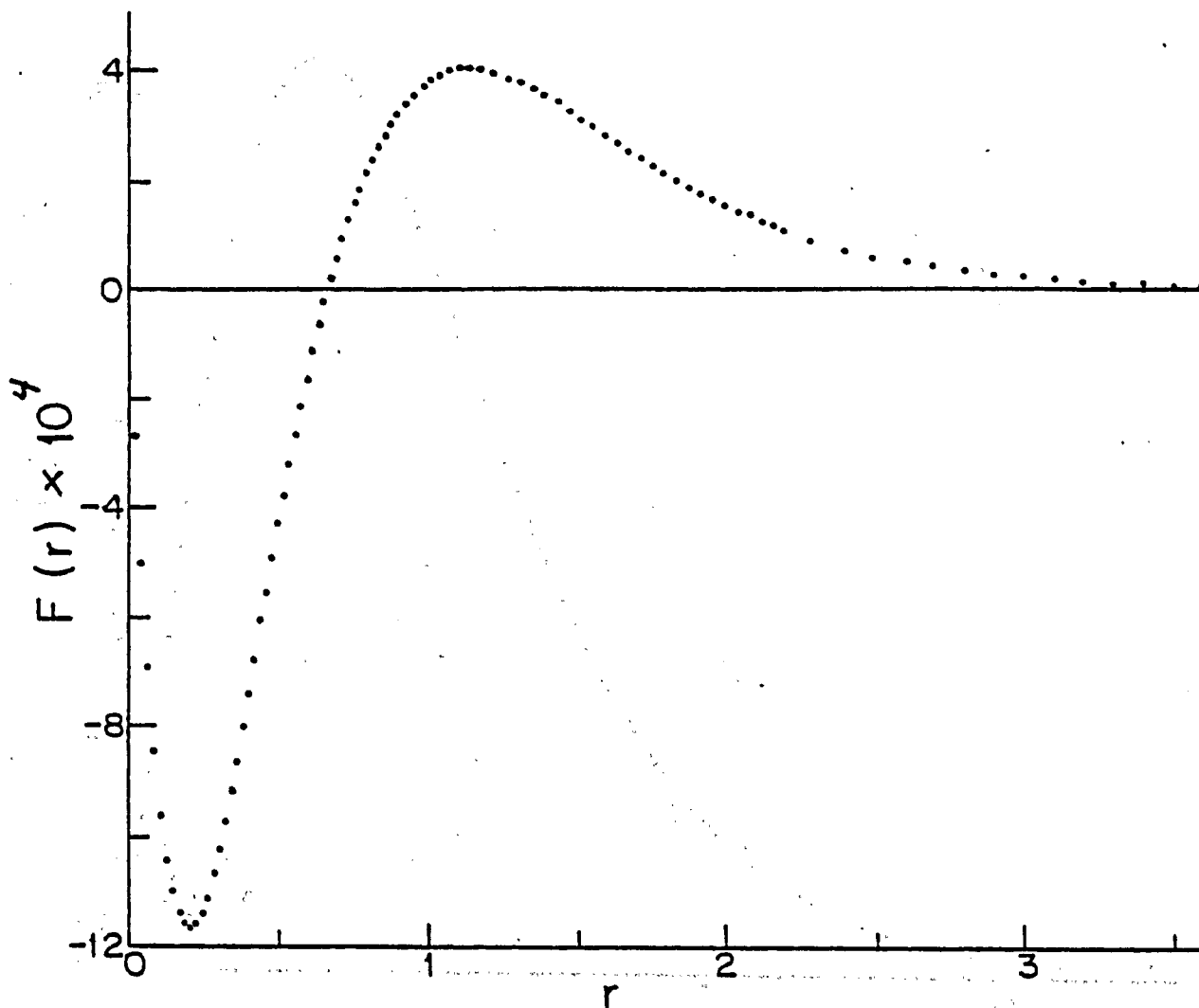


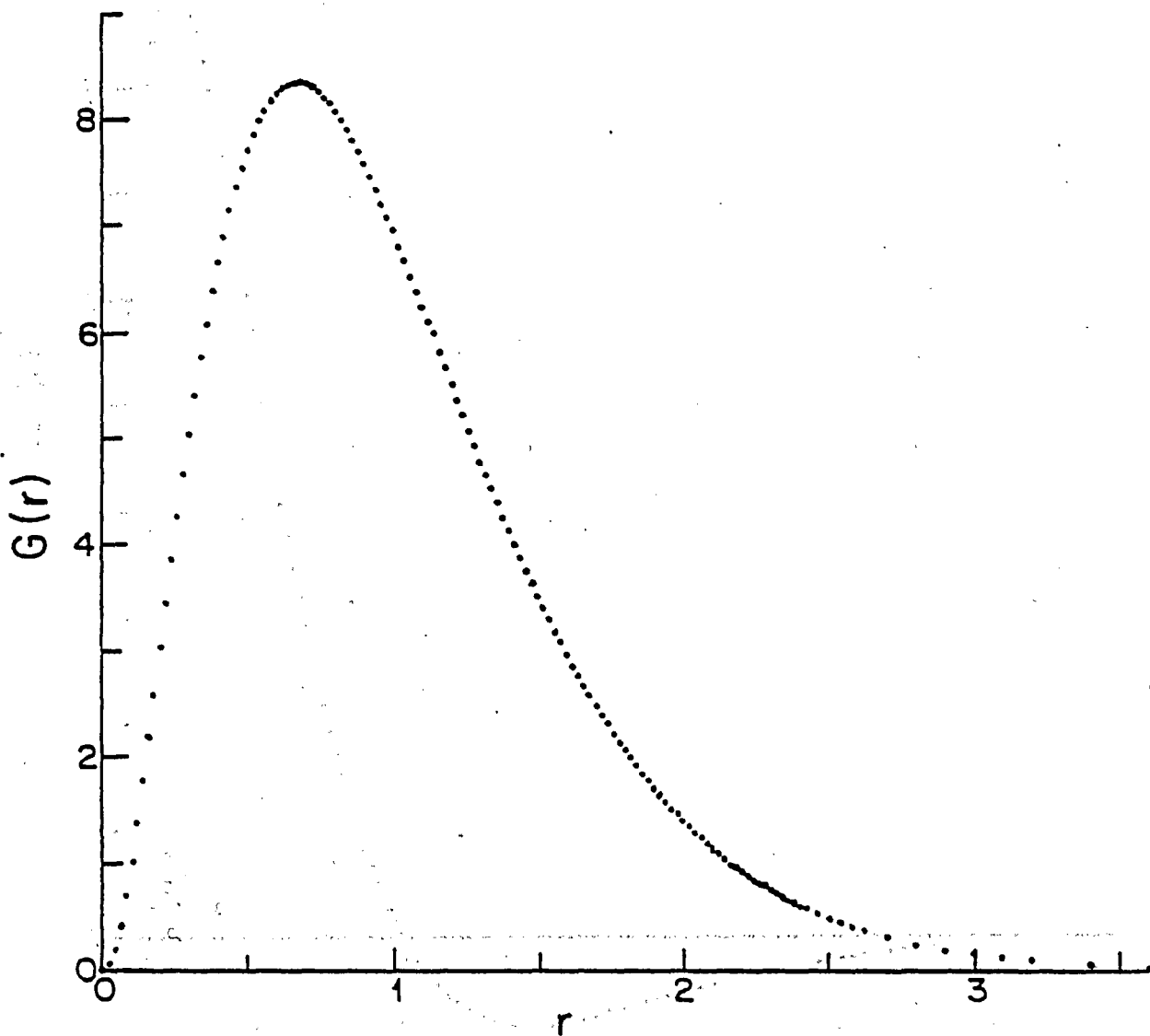
Be<sub>7</sub> 2s<sub>3/2</sub> Unnormalized G(r) vs r

A = 9.95

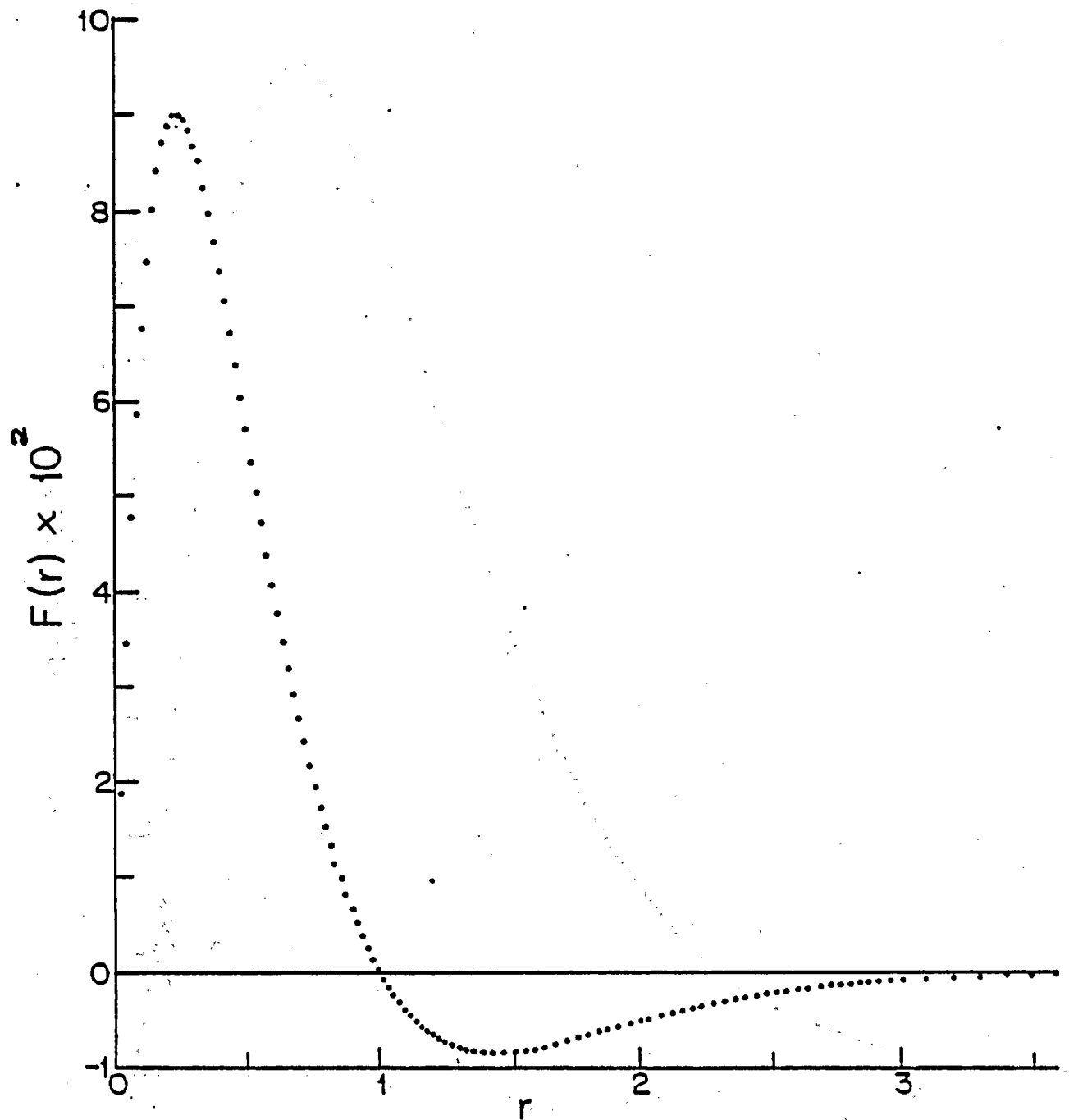


Eq. 25<sub>2</sub> Unnormalized  $F(r)$  vs  $r$

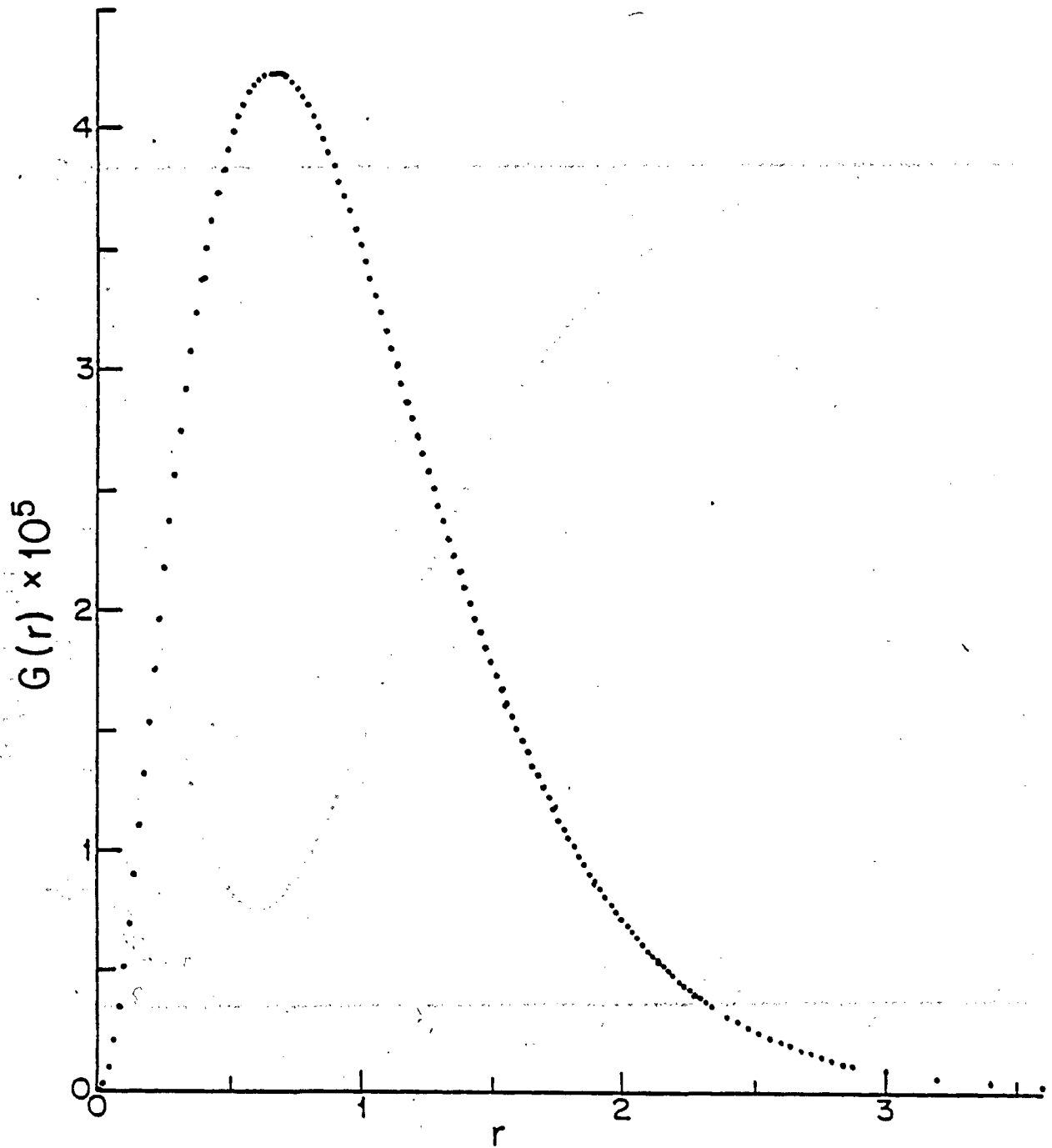


Be<sub>9</sub> 2p<sub>z</sub> Unnormalized G(r) vs rA = .129

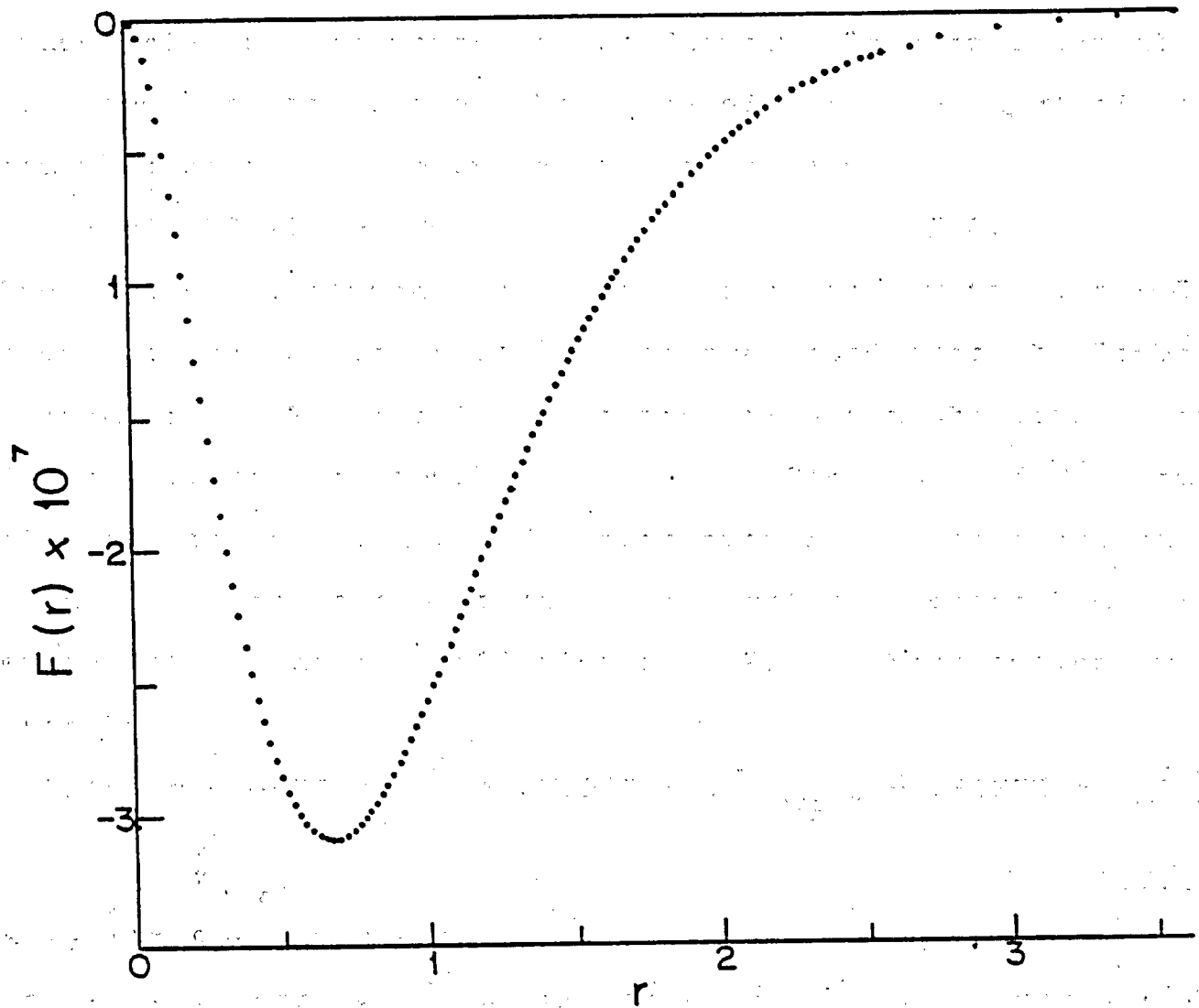
$\text{Be}_9$   $2p_{3/2}$  Unnormalized  $F(r)$  vs  $r$



Be  $2p_{3/2}$  Unnormalized  $G(r)$  vs  $r$



Be  $2p_{3/2}$  Unnormalized  $F(r)$  vs.  $r$



3.2 Computational Procedures and Error Discussions

Romberg integration and Aitkens interpolation proved useful as a check on the application of the expansion given by Huang, and Fullerton and Rinker for the  $\alpha Z\alpha$  and  $\alpha^2 Z\alpha$  vacuum polarization potentials. Further, Romberg integration was used to calculate the value of  $f(x)$  in  $R_{21}(x)$  of the vacuum polarization potential giving a value

$$\int_0^1 f(x) dx \approx 2.468 \pm .001 \quad (3.2.1)$$

Also, the perturbation calculation involving the  $\alpha^2 Z\alpha$  vacuum polarization potential was evaluated through Romberg integration. Numerical integration afforded the possibility of producing a rough curve fit for the  $\alpha^2 Z\alpha$  vacuum polarization potential. Two such curves were constructed in different regions using the method described for interpolation using coefficients (A.2). These curves were given by

$$R_{21}(r) \approx -.4932 \times 10^{-8} + .28602 \times 10^{-6} \frac{e^{-r}}{(2r)^{1/2}} + .80975 \times \frac{10e^{-3r}}{2r} \quad (3.2.2)$$

where  $1.5 < r \leq 2.5$  and

$$R_{21}(r) \approx -.31525 \times 10^{-9} + .611186 \times 10^{-7} \frac{e^{-r}}{2r} + .107982 \times \frac{10e^{-2r}}{2r} \quad (3.2.3)$$

where  $2.5 < r \leq 3.5$ .

The first of these (3.2.2) has a maximum error of about 3%,

whereas the second has a maximum error of about 6%. Because of the smallness of the wavefunction in these regions, the error of the perturbation calculation is much smaller than 6%. In fact the estimated error of the perturbation calculation is less than .3%.

The contribution of the potential for  $r$  greater than 3.5 did not affect the perturbation calculations to within the desired degree of accuracy. The normalization

$$\langle \psi | \psi \rangle = \int_0^{\infty} (|F(r)|^2 + |G(r)|^2) dr \quad (3.2.4)$$

had a truncated upper limit in order to evaluate the integral numerically to within the desired accuracy.

The coupled differential equations 2.2.13 were evaluated numerically for 2 or 3 trial energy eigenvalues and the wavefunctions examined at large  $r$ . The energy eigenvalues were then calculated for the value in which the wavefunctions were 0 at large  $r$ . This was done using either linear or quadratic Aitkens interpolation. The process of solving the differential equations for 2 or 3 energy eigenvalues and interpolating was repeated until the energy eigenvalues were of the desired accuracy. The starting point for the energy calculations was the non-relativistic eigenvalue.

$$E = \frac{-\frac{1}{2} \alpha^2 m_r}{2n^2} \quad (3.2.5)$$

after which the rest energy  $m_r$  was added. Errors in solving the differential equations for the energy were estimated by

varying the truncation error tolerance and/or the distance of integration while observing the effect on the energy eigenvalues.

The curve fits for  $H_1$  and  $H_2$  were estimated to be accurate to approximately .5%. For  $He_4$  the estimated error was approximately .25%. In addition to the numerical errors indicated for the  $Li_6$  and  $Be_9$   $\alpha Z\alpha$  vacuum polarization and finite nuclear size corrections, the error due to using a homogeneous charge distribution for the vacuum polarization potential was estimated (see Table 3.1.7). This error was estimated at approximately 3 in the fourth figure for  $Li_6$  and 1 in the third figure for  $Be_9$ . Due to the large dependence on  $r$  of  $E(2s_{\frac{1}{2}} - 2p_{\frac{1}{2},\frac{3}{2}})$  for  $Li_6$  and  $Be_9$ , these curve fits were still estimated to be accurate to approximately .5%.

### 3.3 Discussion of Results:

The results show that some transition frequencies lie in the visible region of the spectrum. It is well known that the  $2s_{1/2} - 2p_{1/2}$  and  $2s_{1/2} - 2p_{3/2}$  transition frequencies for  $\mu^-$ -He<sub>4</sub><sup>++</sup> lie in or near the visible region of the spectrum. The present calculations show that the transitions  $2s_{1/2} - 2p_{3/2}$  in  $\mu^-$ -Li<sub>3</sub><sup>+</sup> and  $2s_{1/2} - 2p_{1/2}$  in  $\mu^-$ -Be<sub>9</sub><sup>4+</sup> also lie in or near the visible region (Table 3.1.5). At first sight this result is surprising because one would normally expect the transition frequencies to scale as  $Z^4$ . A study of the order of magnitudes for the vacuum polarization and finite size corrections (2.10) shows that as  $Z$  increases the finite size correction, initially smaller, eventually dominates the vacuum polarization correction. The reason that the transition frequencies are so small for the above cases is that the vacuum polarization and finite size corrections are of similar magnitude and act in opposite directions causing strong cancellation. Further, the dominance of the finite size correction is easily seen in Table 3.1.5 by noting the change of sign from Li<sub>3</sub> to Be<sub>9</sub> of the  $2s_{1/2} - 2p_{1/2}$  energy splitting.

The strong nuclear radial dependence of these Lamb shifts is the result of the relative importance of the finite size correction to the overall Lamb shift. Due to the

strength of the nuclear radial dependence, empirical curve fits relate the  $2s_{1/2} - 2p_{1/2, 3/2}$  energy differences to the nuclear radius with fairly good accuracy (see 3.2).

#### 4 Conclusions and Discussions

As the results have indicated, the quantum electrodynamic effects in low  $Z$  muonic atoms were pronounced. The energy differences  $2s_{\frac{1}{2}} - 2p_{\frac{1}{2}, \frac{3}{2}}$  displayed Q.E.D. effects due to nuclear vacuum polarization and muon self energy. Also the finite size correction to Lamb shifts was seen to be of increasing importance with increasing  $Z$ , eventually dominating the correction due to vacuum polarization. The finite size correction in the  $2s_{\frac{1}{2}} - 2p_{\frac{1}{2}}$  and  $2s_{\frac{1}{2}} - 2p_{\frac{3}{2}}$  energy splittings for  $Z \gg 4$  and  $Z \gg 5$  respectively was seen to be the dominant correction.

The mode and/or feasibility for future muonic Lamb shift measurements is also seen by the results. These results show (based on current nuclear radii) that Lamb shifts for  $\text{He}_4^{++}$  lie just outside the visible spectrum toward the infra red region. The same is true for  $\text{Be}_9$  for the  $2s_{\frac{1}{2}} - 2p_{\frac{1}{2}}$  energy difference. The  $2s_{\frac{1}{2}} - 2p_{\frac{3}{2}}$  energy difference for  $\text{Li}_6$  lies in the visible spectrum. The other values lie in the infra red region. The ranges of wavelengths given in 3.1.5 are covered by a variety of tunable laser types. Among these are dye lasers ( $\sim 3000 \text{ \AA} - \sim 10,000 \text{ \AA}$ ), semiconductor lasers ( $\sim 5000 \text{ \AA} - \sim 300,000 \text{ \AA}$ ), colour centre lasers ( $\sim 11,000 \text{ \AA} - \sim 30,000 \text{ \AA}$ ), Raman lasers ( $\sim 1500 \text{ \AA} - \sim 10,000 \text{ \AA}$ ) in addition to optical mixing techniques ( $\sim 1000 \text{ \AA} - 10^6 \text{ \AA}$ ).

Since the nuclear radius is not known to better than a few percent in  $\text{Li}_\mu$  and  $\text{Be}_\mu$ , it is very possible that Lamb shifts which appear to lie in the infra red region may actually lie in the optical region. An examination of the data for  $\text{Be}_\mu$  gives the wide range of possible values for  $\Delta E(2s_{1/2} - 2p_{1/2, 3/2})$  for small variations of the nuclear radius.

The strong nuclear radial dependence of Lamb shifts in muonic atoms allows for an accurate determination of the nuclear radius by comparing the calculated energy splittings with future measurements. These nuclear radii may in turn be used to calculate the finite size correction in electronic Lamb shifts. By removing the finite size corrections from measured Lamb shifts of electronic atoms, higher order Q.E.D. corrections can be verified.

Concerning actual calculations, the ability to obtain energy levels by numerical integration of the Dirac equation has advantages over calculating corrections through first order perturbation theory. Firstly, the contribution of each potential to energy levels is more accurately determined by the calculation of the associated energy eigenvalues. This result is obvious as first order perturbation only includes the first two terms of a perturbation expansion. Secondly, any combination of potentials may be included directly into the Dirac equation rather than performing several

perturbation calculations.

The largest neglected contributions to the Lamb shifts are the nuclear polarization correction and the replacement of an exponential charge distribution in the  $\propto Z\alpha$  nuclear vacuum polarization potential. These account for about .3% error in the Lamb shifts. However, since the nuclear radial dependence is so strong in  $Li_6$  and  $Be_9$ , the error in the nuclear radius due to these corrections can be estimated at less than .1%. Including these corrections in the Lamb shifts and using least square fits would allow the nuclear radius to be determined to better than .1% in  $Li_6$  and  $Be_9$ .

## Appendix A

### Numerical Techniques

This section gives the background for the numerical techniques and computational procedures used in this work. There are three numerical techniques which proved useful. Romberg's method of integration, which is useful in evaluating potentials, is described in section A.1. Another technique useful in curve fits and energy calculations is interpolation, discussed in section A.2. Section A.3 explains numerical techniques used in solving the Dirac equation. Section 3.2 described how the computational procedures were applied for obtaining the energy levels, splittings and curve fits.

#### A.1 Romberg Integration

Romberg integration provides a rapidly converging method of numerical integration. The method uses successive iterations to reduce the error term in the previous iteration, the starting point being the trapezoidal rule.

Consider the trapezoidal rule and its error

$$E = I_p^{(h)} - I_p^{(o)} \quad (\text{A.1.1})$$

where  $I_p^{(h)}$  is the actual integral up to order  $h^2$  and  $I_p^{(o)}$  is the value obtained by the trapezoidal rule. Since the error for the trapezoidal rule behaves as  $h^2$ , halving the step size gives 1/4 the error. Thus from A.1.1

$$I_{p-1}^{(1)} = E_{p-1} + I_{p-1}^{(0)} \quad (\text{A.1.2})$$

and

$$I_p^{(1)} = E_p + I_p^{(0)} = \frac{1}{4}E_{p-1} + I_p^{(0)} \quad (\text{A.1.3})$$

give

$$I_p^{(1)} = \frac{4I_p^{(0)} - I_{p-1}^{(0)}}{3} \quad (\text{A.1.4})$$

Continuing in exactly the same manner to eliminate the errors of order  $h^4, h^6, \dots$ , the value for  $m$  iterations is given by

$$I_p^{(m)} = \frac{4I_p^{(m-1)} - I_{p-1}^{(m-1)}}{4^m - 1} \quad (\text{A.1.5})$$

## A.2 Interpolating Polynomials

(a) An interpolating polynomial is a method of determining functional values where the function is not given explicitly. The function is approximated by a polynomial

$$f(x) \approx p(x) = \sum_{k=0}^n a_k x^k, \quad (\text{A.2.1})$$

where there are  $n+1$  points for which

$$f(x_i) = p(x_i) \quad i = 0, 1, \dots, n \quad (\text{A.2.2})$$

are known. The coefficients of  $p(x)$  are then determined by solving the  $n+1$  equations in  $n+1$  unknowns given by A.2.1 and A.2.2. Thus for

$$A = \{x_0, x_1, \dots, x_n\} \quad (\text{A.2.3})$$

$f(x)$  may be approximated by  $p(x)$  for  $x$  in  $[min A, max A]$ . Extrapolation may also be done for short intervals outside

[min A, max A].

(b) A useful interpolating technique which evaluates a function up to an  $n^{\text{th}}$  order polynomial (depending on the desired accuracy) is given by Aitkens interpolation method.

Define

$$P_{x_0, x_1, \dots, x_n}^k(x) = \frac{1}{x_n - x_0} \begin{vmatrix} x - x_0 & P_{x_0, x_1, \dots, x_{n-1}}^{k-1}(x) \\ x - x_k & P_{x_1, x_2, \dots, x_n}^{k-1}(x) \end{vmatrix} \quad \text{---} \quad \text{(A.2.4)}$$

where

$$P^0(x_i) = f(x_i) \quad \text{(A.2.5)}$$

A table for the iterative procedure is given below

Table A.1

Iterations

	0	1	2	...	n
$x_0$	$f(x_0)$				
		$P_{x_0, x_1}^1(x)$			
$x_1$	$f(x_1)$		$P_{x_0, x_1, x_2}^2(x)$		
		$P_{x_1, x_2}^1(x)$			
			$\vdots$		$P_{x_0, x_1, \dots, x_n}^n(x)$
		$P_{x_{n-1}, x_n}^n(x)$	$P_{x_{n-2}, x_{n-1}, x_n}^2(x)$		
$x_n$	$f(x_n)$				

Each iteration produces a polynomial of the order of the number of iterations, the value being reflected along the upper descending diagonal of Table A.1. This may easily be seen by substituting the appropriate values for  $p$  in terms of  $x$  and  $f(x_i)$  in A.2.2. Since

$$p(x_i) = f(x_i) \quad \text{for } i=0,1,2,\dots,k, \quad (\text{A.2.6})$$

the polynomial is uniquely determined and the value of  $f(x)$  for  $x$  in  $[\min A, \max A]$  is approximated by it.

### A.3 Numerical Solutions to First Order Coupled Differential Equations

The numerical method used to solve differential equations involves three Gill-Runge-Kutta steps followed by a Hamming's predictor-corrector. The Gill-Runge-Kutta steps are based on the Taylor series expansion

$$y(x_{i+1}) = y(x_i) + hy'(x_i) + \frac{h^2}{2!} y''(x_i) + \dots \quad (\text{A.3.1})$$

where

$$h = (x_{i+1} - x_i). \quad (\text{A.3.2})$$

Consider

$$y(x_{i+1}) = y(x_i) + \frac{1}{2} \left[ k_1 + 2\frac{(1-1)}{\sqrt{2}}k_2 + 2\frac{(1+1)}{\sqrt{2}}k_3 + k_4 \right] \quad (\text{A.3.3})$$

where

$$k_1 = hf(x_i, y_i)$$

$$k_2 = hf(x_i + \frac{h}{2}, y_i + \frac{k_1}{2})$$

$$k_3 = hf(x_i + \frac{h}{2}, y_i + (1-\frac{1}{\sqrt{2}})k_2 - \frac{(1-\frac{1}{\sqrt{2}})k_1}{\sqrt{2}})$$

$$k_4 = hf(x_i + h, y_i + (1+\frac{1}{\sqrt{2}})k_3 - \frac{1}{\sqrt{2}}k_2)$$

$$y' = f(x, y). \tag{A.3.4}$$

A.3.1 and A.3.3 are equivalent to fourth order in h, as can be revealed by expanding  $k_1, k_2, k_3, k_4$  in A.3.3 in two dimensional Taylor series and retaining terms to order  $h^4$ .

Using the initial value and the three Gill-Runge-Kutta steps, the four required points for the Hamming's predictor-corrector are applied. The Hamming's predictor is based on the four points contained in the expression

$$y_{i+1} = y_{i-3} + \frac{4h}{3}(2y'_i - y'_{i-1} + 2y'_{i-2}) \tag{A.3.5}$$

In order to obtain A.3.5 consider

$$\begin{aligned} \phi'(x) = & y'_n + \frac{y'_n - y'_{n-1}}{h} (x-x_n) + \frac{y'_n - 2y'_{n-1} + y'_{n-2}}{2!h^2} (x-x_n)(x-x_{n-1}) \\ & + \frac{y'_n - 3y'_{n-1} + 3y'_{n-2} - y'_{n-3}}{3!h^3} (x-x_n)(x-x_{n-1})(x-x_{n-2}) \end{aligned} \tag{A.3.6}$$

It is clear that

$$\phi'(x_{n-k}) = y'_{n-k} \quad k = 0, 1, 2, 3. \tag{A.3.7}$$

Using

$$y(x_{n+1}) - y(x_{n-3}) = \int_{x_{n-3}}^{x_{n+1}} y'(x) dx, \tag{A.3.8}$$

approximating  $y'(x)$  to third order by  $\phi'(x)$  in A.3.8 yields

$$y(x_{n+1}) - y(x_{n-3}) \approx \int_{x_{n-3}}^{x_{n+1}} \phi'(x) dx. \tag{A.3.9}$$

Substituting  $\phi'(x)$  from A.3.6 and integrating A.3.9 gives  
 A.3.5. The general corrector is given by

$$y_{n+1} = a_n y_n + a_{n-1} y_{n-1} + a_{n-2} y_{n-2} + h(b_{n+1} y'_{n+1} + b_n y'_n + b_{n-1} y'_{n-1}). \tag{A.3.10}$$

Setting  $a_{n-1} = 0$ , expanding the left and right hand sides of A.3.10 and adjusting the remaining coefficients so that the left and right hand sides are equivalent up to order  $h^4$  gives

$$y_{n+1} = \frac{1}{8} [9y_n - y_{n-2} + 3h(y'_{n+1} + 2y'_n - y'_{n-1})] - \frac{1}{40} h^5 y^{(5)}(\xi) \tag{A.3.11}$$

A modifier is based on the truncation error and it is given by

$$m_{n+1} = p_{n+1} - \frac{112}{121} (p_n - c_n), \tag{A.3.12}$$

an improved value for  $y_{n+1}$ . The corrector is given by A.3.11 where we replace  $y'_{n+1}$  with  $m'_{n+1}$ . The truncation error of the corrector is given by

$$E = \frac{9}{121} (p_n - c_n), \tag{A.3.13}$$

hence

$$y_{n+1} \approx c_n + \frac{9}{121} (p_{n+1} - c_{n+1}). \tag{A.3.14}$$

REFERENCES

1. W.E. Lamb Jr. and R.C. Retherford, Phys. Rev. 72, 241 (1947).
2. W.E. Lamb Jr. and R.C. Retherford, Phys. Rev. 79, 549 (1950).
3. W.E. Lamb Jr. and R.C. Retherford, Phys. Rev. 81, 222 (1951).
4. W.E. Lamb Jr. and R.C. Retherford, Phys. Rev. 96, 1014 (1952).
5. G. Newton, D.A. Andrews, and P.J. Unsworth, Philos. Trans. R. Soc. London 290, 373 (1979).
6. S.R. Lundeen and F.M. Pipkin, Phys. Rev. Lett. 46, 232 (1981).
7. G.W.F. Drake, Phys. Rev. A, 19, 1387 (1979).
8. O.R. Wood II, C.K.N. Patel, D.E. Murnick, E.T. Nelson, M. Leventhal, H.W. Kugel and Y. Niv, Phys. Lett. 48, 398 (1982).
9. A. Bertin, G. Carboni, J. Duclos, U. Crastaldi, G. Gorini, G. Neri, J. Picard, O. Pitzurra, A. Placci, E. Polacco, G. Torelli, A. Vitale, and E. Zavattini, Phys. Lett. B 55, 411 (1975).
10. G. Carboni, G. Gorini, G. Torelli, L. Palffy, F. Palmonari, and E. Zavattini, Nucl. Phys. A 278, 381 (1977).
11. G. Carboni, G. Gorini, E. Iacopini, L. Palffy, F.

11. G. Carboni, G. Corini, E. Iacopini, L. Palffy, F. Palmonari, G. Torelli and E. Zavattini, Phys. Lett. B 73, 229 (1978).
12. A. Di Giacomo, Nucl. Phys. B 11, 411 (1969).
13. E. Borie and G.A. Rinker, Rev. Mod. Phys 54, No.1, 67 (1982).
14. A. Messiah, Quantum Mechanics (Wiley, New York, 1961).
15. G.A. Rinker, Physical Review A 14, No. 1, 14 (1976).
16. J. Bjorken and S. Drell, Relativistic Quantum Mechanics (McGraw-Hill, New York, 1964).
17. A.I. Akhiezer and V.B. Berestetskii, Quantum Electrodynamics, (Wiley, New York, 1965).
18. K.N. Huang, Physical Review A 14, 4, 1311 (1976).
19. L.W. Fullerton and G.A. Rinker Jr., Phys. Rev. A 13, 3, 1283 (1976).
20. G.W.F. Drake, Advances in Atomic and Molecular Physics, 18, (1982).
21. A. Ralston ed., Mathematical Methods For Digital Computers, (Wiley, New York, 1960).
22. H.A. Bethe and E.E. Salpeter, Quantum Mechanics of One- And Two-Electron Atoms, (Academic Press, New York, 1957).
23. S.G. Kellison, Fundamentals of Numerical Analysis, (Richard D. Irwin Inc., Illinois, 1975).

24. L.D. Landau and E.M. Lifshitz, Quantum Electrodynamics, (Pergamon, Toronto, 1982).

25. Wolfgang Demtroder, Laser Spectroscopy-Basic Concepts and Instrumentation, (Springer-Verlag, New York, 1981).

100001

900800

VITA AUCTORIS

Louis Lee Byer was born on May 13, 1957; he completed high school at Centennial Secondary School in Windsor and obtained a B.Sc. degree from McMaster University in Hamilton. In the Fall of 1981 he began a Master's program in Physics at the University of Windsor and expects to graduate in the Spring of 1984.